END

FILMED

DTIC

MICROCOPY RESOLUTION TEST CHART

NATIONAL BUREAU OF STANDARDS-1963-A

STUDIES OF STRUCTURE AND MODELING IN TURBULENT SHEAR FLOWS

by

Joel H. Ferziger
O.J. McMillan

DTIC
ELECTE
MAR 1 8 1985
S

NIELSEN ENGINEERING
AND RESEARCH, INC.

85 08 06 004

STUDIES OF STRUCTURE AND MODELING
IN TURBULENT SHEAR FLOWS

by

Joel H. Ferziger
O.J. McMillan

NEAR TR 335
December 1984

DTIC
ELECTE
MAR 1 8 1985
S D
A

NIELSEN ENGINEERING & RESEARCH, INC.
510 Clyde Avenue, Mountian View, CA 94043
(415) 968-9457

REPORT DOCUMENTATION PAGE	READ INSTRUCTIONS BEFORE COMPLETING FORM

1. REPORT NUMBER	2. GOVT ACCESSION NO.	3. RECIPIENT'S CATALOG NUMBER
	AD-A151 807	

4. TITLE (and Subtitle)	5. TYPE OF REPORT & PERIOD COVERED
Studies of Structure and Modeling in Turbulent Shear Flows	Final Report 15 July, 1982-30 September, 1984
	6. PERFORMING ORG. REPORT NUMBER
	NEAR TR 335

7. AUTHOR(s)	8. CONTRACT OR GRANT NUMBER(s)
Joel H. Ferziger O.J. McMillan	N00014-82-C-0672

9. PERFORMING ORGANIZATION NAME AND ADDRESS	10. PROGRAM ELEMENT, PROJECT, TASK AREA & WORK UNIT NUMBERS
NIELSEN ENGINEERING & RESEARCH, INC. 510 Clyde Avenue, Mountain View, CA 94043	

11. CONTROLLING OFFICE NAME AND ADDRESS	12. REPORT DATE
Office of Naval Research Arlington, VA 22217	December, 1984
	13. NUMBER OF PAGES
	55 pages

14. MONITORING AGENCY NAME & ADDRESS(if different from Controlling Office)	15. SECURITY CLASS. (of this report)
	Unclassified
	15a. DECLASSIFICATION/DOWNGRADING SCHEDULE

16. DISTRIBUTION STATEMENT (of this Report)

Approved for public release.
Distribution unlimted.

17. DISTRIBUTION STATEMENT (of the abstract entered in Block 20, if different from Report)

18. SUPPLEMENTARY NOTES

19. KEY WORDS (Continue on reverse side if necessary and identify by block number)

Turbulence Modeling

20. ABSTRACT (Continue on reverse side if necessary and identify by block number)

Several issues connected with turbulence and its modeling were studied using the results of full simulations of homogeneous turbulent flows. It was found that the mechanism of turbulence production in homogeneous sheared turbulence resembles the mechanism of the turbulence production in the mixing layer. It appears that it is possible to fit a wide range of shear flows, which have greatly different physical behavior, with a single ———

DD FORM 1473 1 JAN 73 EDITION OF 1 NOV 65 IS OBSOLETE

turbulence model. A study of length scales used in turbulence modeling revealed that they are dependent on Reynolds number and the ratio of production to dissipation. Model parameters need to be different for each class of flow, sheared turbulence, plane strain, and axisymmetric strain flows. A principal recommendation resulting from this study is that full turbulence simulations should be used when feasible for the purpose of studying both the physics of turbulence and turbulence modeling. Combination of simulation data with experimental data would be even more desirable. Development of new methods of investigating the data should be encouraged.

TABLE OF CONTENTS

NOMENCLATURE

C_u — Eddy viscosity coefficien. (Eq. 3).

$C_{1_\epsilon}, C_{2_\epsilon}$ — Coefficients of dissipation equation (Eq. 8).

k — Turbulence kinetic energy per unit mass, $\frac{1}{2}(u_1'^2 + u_2'^2 + u_3'^2)$.

$L_{11,2}$ — Integral length scale (eq. 1).

ℓ, L — Length parameters.

ℓ_ϵ — Dissipation length scale.

ℓ_{mix} — Mixing length.

P — Rate of production of turbulence kinetic energy.

q — A velocity associated with turbulence.

R_e — Reynolds number.

R_{11} — Two-point autocorrelation of streamwise velocity.

S — Strain.

S_{ij} — Components of strain tensor (Eq. 2).

St — Total strain = strain x time.

t — Time.

u' — Components of velocity fluctuations; $i = 1,2,3$.

U — Components of total velocity $U_i = \overline{U}_i + u_i'$; $i = 1,2,3$

x_i — Cartesian Coordinate; $i = 1,2,3$.

ϵ — Rate of dissipation of turbulence kinetic energy.

ν_t — Eddy viscosity

SPECIAL NOTATION

$\overline{(\quad)}$ — Denotes a time-averaged value.

1. Introduction

Until the past twenty years, turbulence was thought to be
totally chaotic. Most early approaches to understanding and
predicting turbulent flows were statistical in nature. In them,
statistically steady turbulent flows were considered
superpositions of time mean velocity profiles and random
fluctuations about those means. Although this approach has had
notable successes, the goal of finding a single method capable of
simulating all, or at least a wide range, of turbulent flows has
proved elusive. This may indicate that the concepts embodied in
the statistical approach do not provide a complete description of
the phenomena occuring in turbulent flows.

In the last twenty years, it has become clear that coherent
or organized structures and events not only occur in turbulent
flows but are probably responsible for many of the important
properties of these flows. In particular, organized structures
are now thought to account for a large fraction of the mass,
momentum, and energy transport and production of new turbulent
motions. Indeed, a reasonable picture of a turbulent flow may be
one in which coherent structures or events containing a small
fraction of the velocity fluctuations are responsible for much of
the property transport. On the other hand, in this picture,
incoherent motions make up the bulk of the fluctuating field but
account for only a small fraction of the transport. However, the
incoherent motions mask the coherent events, making them
difficult to find in the laboratory; this may be the reason why
they remained undiscovered for so long.

This picture of turbulence, if correct, indicates that the
events occuring in turbulent flows may be flow dependent.
Consequently, it may not be possible to treat all turbulent flows
with a single model containing a small number of empirical

constants or functions. Turbulence models of the future may need
to reflect the physics of each particular region of a flow i.e.
they may need to be different in each region, or zonal in nature.

The work reported herein attempts to resolve some questions
raised by this picture of turbulent flows. The approach is to
simultaneously look at a turbulent flow with statistical and
visualization techniques. Statistical methods provide the
quantities contained in nearly all currently used turbulence
models while visualization methods are the best known means of
revealing the coherent structures. To carry out such a program,
one needs detailed velocity field data. The best source of such
data at present is full simulations of turbulent flows, which are
available for only a few simple flows. Because the required data
were available for them, we decided to concentrate on homogeneous
turbulent flows in this study. These flows may be structurally
different from flows of technological interest, but their
simplicity makes them easier to study. It is also easier to test
ideas about turbulence and its modeling on these flows. In
particular, we shall study whether a single model (including a
single set of constants) can be applied to a variety of
homogeneous turbulent flows visually with the aim of determining
whether the mechanisms of turbulent transport and production in
them are similar to those in inhomogeneous flows.

In the usual view of turbulent flows, the phenomena to be
modeled are the production of new turbulent fluctuations, the
redistribution of energy among the components of the turbulence,
viscous dissipation, and diffusion. In homogeneous turbulence,
all statistical average quantities are independent of position so
diffusion does not occur. The production terms are not modeled
in any flow and so, never require special attention. The
redistribution terms, to which the fluctuating pressure makes a
large contribution, have been studied extensively by other

-2-

authors including Feiereisen et al (1981), Shirani et al (1981), and Rogallo (1981); we are not in position to add significantly to their contributions. For these reasons, the statistical part of this study will concentrate on the modeling of the length scales and the dissipation. Our decision to study these was reinforced by the general impression that these are the weakest points in current turbulence models.

The plan of this report is as follows. In the next chapter, we shall use the results of full simulations of homogeneous turbulent shear flow to look for evidence of the turbulence production mechanisms that are known to exist in inhomogeneous shear flows. The object is to discover similarities and differences between the two types of flows with the goal of shedding light on the question of whether one can expect the same model to deal with both types of flow. We find that the structures in the two flows are different; the mechanism of turbulence production in the homogeneous flow appears to be more akin to that of the inner region of the boundary layer than to that of the inhomogeneous shear layer.

In Chapter 3, we shall look at the length scales of turbulence in homogeneous flows including both shear flow and two kinds of irrotational strain flow. The objective is to determine how well the models match the actual length scales in the homogeneous flows.

Turbulence models, especially the currently popular two-equation models, use the dissipation of turbulence energy as a means of determining the length scale. The models used in the dissipation equation are generally considered more suspect than those used in the kinetic energy equation. Accordingly, we shall look at the models used in the dissipation equation in Chapter 4 to determine whether a model with a single set of constants can be applied to all of these flows. The results can be regarded as evidence as to whether one model can serve for a variety of flows

in the more general case. We shall find that the constants do require variation from flow to flow.

The data used in this study were taken from the full simulations of homogeneous turbulence made by Rogallo (1981) and Lee and Reynolds (1984); they provided data for which the authors of this report are grateful. The raw data are given in Tables 1-3.

2. Structure in Homogeneous Shear Flow

Experimental evidence accumulated in the past ten years shows that the energetic behavior of the turbulent mixing layer (including its rapid growth) can be explained by deterministic mechanisms. The best known mechanism is merging of two or more vortices to form a larger vortex; when two vortices are involved in this process, it is called pairing (Brown and Roshko, 1974, Winant and Browand, 1974). Another mechanism is tearing in which a vortex is torn apart and distributed to its neighbors (Moore and Saffman, 1975).

The pairing mechanism is most clearly displayed in two dimensional flows in which the merging vortex tubes are straight. However, the vortex tube structures seem to be unstable with respect to three dimensional perturbations that destroy their spanwise coherence. In particular, if a vortex develops spanwise waviness, parts of it may pair with the vortex ahead of it while other parts pair with the vortex behind it. This process has been called local or helical pairing and was observed in simulations by Cain et al (1981) and predicted theoretically by Pierrehumbert and Widnall (1982). It produces a three dimensional flow in which the pairing process is important but not spanwise coherent. Another mechanism for producing three dimensionality is the production of streamwise vorticity by the stretching vortices. This process was observed in the laboratory by Konrad (1976) and in simulations by Cain et al (1981) and explained theoretically by Corcos and Lin (1984).

-4-

The mechanism of turbulence production in boundary layers is quite different and not totally understood. In part, it involves lifting of slow-moving vorticity-containing fluid from the wall. As this fluid rises into the faster moving parts of the flow the vorticity it contains is stretched; the result is 'hairpin' vortices. The hairpin vortices induce lift up of other vortices from the surface. The combination of lifting and stretching produces vertically oriented thin shear layers across which there are strong gradients of the streamwise component of the velocity. These shear layers then break down to form chaotic motions. The entire process involves a great deal of momentum transport and, therefore, Reynolds stress. The process was described in detail by Kline et al (1967).

Homogeneous turbulent flows are often used as building blocks in the development of turbulence models. Since we have argued that turbulence models should reflect flow structure and that different models may be needed for regions with different kinds of structure, it is important to know whether homogeneous flows are like their inhomogeneous counterparts. For this reason, we decided to look for evidence of the mechanisms found in inhomogeneous shear flows in homogeneous shear flow. To accomplish this aim, we need some means of detecting the mechanism of turbulence production.

ʳn the two dimensional mixing layer described above, the Reynolds stress occurs in the regions between merging vortices and is coherent across the span of the flow. In three dimensional flows, such as that of Chandrsuda et al (1978), the velocity correlations still extend two or three layer thicknesses in the spanwise direction. This leads to a picture of these flows as containing 'watermelon' or 'cigar' shaped vortices. Although the process has not been observed in the laboratory, it is likely that these vortices interact in ways similar to those observed in the two dimensional flow i.e. by merging and pairing.

The search for structural coherence in the computed homogeneous shear flows was carried out by constructing contour plots of the instantaneous Reynolds stress and vorticity; an interesting result is found. Figures 1 and 2 show the contours of the Reynolds shear stress on two perpendicular planes at a particular instant in a homogeneous shear flow; there is one region of high Reynolds stress concentration which appears in both views. This region does not have the 'watermelon' shape that would be expected if the homogeneous flow is similar to the mixing layer; instead, it is approximately disc shaped. That is, it is roughly circular in the x-y plane (whose normal is spanwise) and thin in the spanwise direction. Although we were able to visualize only a small number of these Reynolds stress concentrations, all of them had this shape. No structures with greater spanwise extent were found. Furthermore, these structures were found to become larger in size and more intense with time but their shape did not change appreciably.

To study these regions in more detail, contour plots of the fluctuating vorticity were made. Figures 3 and 4 demonstrate that the streamwise and normal vorticity is not concentrated at the same locations as the Reynolds stress but a short spanwise distance to either side of them. From these figures, it appears that the vorticity concentrations are inclined at some angle (our guess based on a limited number of observations is 20-25°) with respect to the streamwise direction and lie on either side of the Reynolds stress concentrations. As shown in Figure 5, the fluctuating spanwise vorticity demonstrates no tendency to form concentrations; this is further evidence that pairing plays no significant role in this flow.

These results demonstrate that the pairing is not a significant mechanism in homogeneous shear flow. The pattern seen in the figures is more reminiscent of the structure seen in the near-wall parts of boundary layers; this was described above. The primary mechanism of turbulence production in these

regions involves the lifting of spanwise vorticity from the
surface, and subsequent stretching and formation of thin vertical
shear layers. In this process, the Reynolds stress is
concentrated between the legs of the stretched vortices where the
velocity generated by the legs of the vortex is such as to pump
low velocity fluid upward. This mechanism gives rise to Reynolds
stress containing regions with thin spanwise extent and greater
extent in the other directions. We thus conclude that the
mechanism for turbulence production in homogeneous shear flow is
similar to, but simpler than, the mechanism responsible for
turbulence production in the near-wall region of wall-bounded
flows. Another important difference is that the homogeneous flow
is symmetric with respect to the upward and downward directions
and the mechanism is equally likely to pump fast moving fluid
downward as slow moving fluid upward. This suggests that
homogeneous shear flow may be an excellent tool for studying the
processes that occur in near-wall regions.

The process has been clarified further by the recent work of
Rogers and Moin (1984). They found that the total vorticity
(including the vorticity of the mean flow) lies predominantly at
an angle of 45° with respect to the mean streamlines and is
associated with sinuous inclined vortices which fill a large part
of the flow. These structures are elongated by their self-
induced velocity and that of the mean flow. They induce an
upward flow of low momentum fluid or a downward flow of high
momentum fluid depending on the sense of their rotation and thus
induce regions of significant Reynolds stress concentration. The
shape of the high Reynolds stress regions suggested by this model
are precisely of the type desribed in the preceeding paragraph.

Thus, the structure of a homogeneous shear flow has more in
common with wall bounded flow than mixing layers. Unless a
single model fitting all of these flows can be found (k- ε models
have been used with some success for this purpose), models for
homogeneous shear flow should behave more like those appropriate

to the inner layers of boundary layers than to those used in
mixing layers.

3. Length Scales

3.1 Turbulence Models

All turbulence models in current use require an estimate of
length scale of the turbulence. In this chapter, we shall
investigate some of these models. To test these models, we need
to have available the length scale which the models are intended
to represent. The appropriate length scale in a turbulent flow
is the size of the eddies responsible for the largest part of the
momentum transport. For a turbulent shear flow, in which the
important momentum flux is normal to the direction of the flow,
the appropriate length scale is the integral scale which measures
the normal extent of the correlation of the streamwise velocity:

$$L_{11,2} = \int R_{11}(0,x_2,0)\ dx_2 \tag{1}$$

where R_{11} is the two-point autocorrelation of the streamwise
velocity. In this chapter, we shall again concentrate on the
homogeneous shear flows. The reasons are two-fold: a) shear
flows are the most important flow class in applications, and b)
the data for the homogeneous shear flows cover a much longer
development time than those for other homogeneous flows, thus
allowing a much more complete study.

Before testing the models, let us introduce them. Because
they receive the greatest amount of attention, we shall
concentrate on models which use the Boussinesq eddy viscosity
concept; these approximate the Reynolds stress by:

$$\overline{u_i' u_j'} = -2\nu_\tau S_{ij} = -\nu_\tau(\frac{\partial U_i}{\partial x_j} + \frac{\partial U_j}{\partial x_i}) \tag{2}$$

-8-

where ν_t is the eddy viscosity. Due to its importance in engineering flows, we shall concentrate on the Reynolds shear stress, $\overline{u_1' u_2'}$.

Simple physical arguments, of which the Prandtl mixing length argument is the simplest, lead to expressions for the eddy viscosity of the form:

$$\nu_\tau = C_\mu q \ell \tag{3}$$

where q is a velocity associated with the turbulence, usually taken as the r.m.s. velocity, ℓ is a length scale, and C_μ is a constant.

In mixing length models, the length scale is prescribed in terms of some physical scale of the flow. For free shear flows, it is some fraction of the width of the layer. In boundary layers, a two layer model, which makes the mixing length proportional to the distance from the wall in the near-wall region and proportional to the boundary layer thickness far from the wall, is used. For homogeneous flows, there is no characteristic length scale. Nonetheless, we can use the data to define a mixing length:

$$\ell_{mix} = \sqrt{\overline{u_1' u_2'}} \Big/ dU_1/dx_2 \tag{4}$$

and we shall study its behavior.

In two-equation models, partial differential equations for turbulence quantities are solved along with those for the mean flow. One equation provides the turbulence kinetic energy, k (per unit mass); its square root is the velocity scale needed in Eq. (3). The second equation may describe the behavior of any of a number of other quantities. The standard modeling assumption is that the length scale is related to the dissipation by:

$$\ell_\varepsilon = q^3/\varepsilon \qquad\qquad (5)$$

cf. Tennekes and Lumley (1972).

Expressions for length scales are needed in other current turbulence models, including Reynolds stress models and algebraic stress models. The accuracy with which Eq. (5) models the length scale of Eq. (1) and the accuracy of the modeling used in the dissipation equation are therefore of great interest; the first issue will be studied in this chapter, the second issue will be taken up in the following chapter.

3.2 Behavior of the Length Scales

In this section, we will study the behavior of the integral length scale defined by Eq. (1), which we take as the significant length scale in sheared turbulence, and at models designed to represent it.

Table 4 gives the length scales defined in the preceeding section as functions of time for the four homogeneous shear flow cases; the mixing length defined by Eq. (4), the dissipation length scale of Eq. (5), and the integral scale defined by Eq. (1) are included. Figure 6 presents this data graphically for a single case; the other cases are qualitatively similar and are not shown. The behavior of the integral scale is somewhat erratic in all cases; this is a consequence of computing the integral scale by numerical integration of Eq. (1). The correlation function in the integrand is negative for some values of x_2 so there is considerable numerical cancelation in the integral, making the result susceptible to numerical errors.

Figure 6 shows that the dissipation length scale is approximately proportional to the integral scale while the mixing length behaves quite differently. As noted above, the mixing length model is not appropriate for this flow. An explanation of its behavior can be provided by rearranging Eq. (4) to yield:

$$\frac{\ell_{mix}}{\ell_\epsilon} = \left[\frac{\overline{u_1'u_2'}}{q^2}\right]^{\frac{1}{2}} \frac{\epsilon}{Sq^2} \tag{6}$$

As the ratio $\overline{u_1'u_2'}/q^2$ is approximately constant (0.15) in nearly all shear flows, Eq. (6) shows that the ratio of the mixing length to the dissipation length scale is proportional to Sq^2/ϵ. The latter quantity is both the ratio of the time required for the imposed shear to modify the flow to the time scale of the turbulence and the ratio of production to dissipation. Technological flows cover only a small range of this parameter allowing the mixing length model to be applied to them. Homogeneous flows, on the other hand, cover a much wider range of this parameter, and the mixing length model cannot work as well for them.

As noted above, Fig. 6 demonstrates that the dissipation length scale is approximately proportional to the integral scale. However, this figure also shows the agreement to be only fair, so we attempted to fit the ratio of these length scales to a function of the dimensionless parameters. There are three such parameters in these flows--the total strain, St, the production-dissipation ratio, P/ϵ, and the Reynolds number, R_e; the last is given in Table 4. The best fit was found when the Reynolds number was used as the correlating parameter; the result is shown in Fig. 7. Considerable fluctuation about the curve fit remains, and can be ascribed, at least in part, to the inaccuracy of the integral scale. Nonetheless, there does appear to be a functional relationship and the curve fit shown in the figure can be represented by:

$$\frac{q^3}{\epsilon L} = \frac{10.7\ Re}{Re + 36.5} \tag{7}$$

-11-

This relationship may be of value in two-equation models for the inner region of wall-bounded flows. Note that, although Fig. (7) suggests that the ratio $q^3/\epsilon L$ goes to zero with the Reynolds number, there is nothing in the figure to suggest whether this is correct or not, so caution is urged if this relationship is applied in near-wall regions. Furthermore, the Reynolds numbers shown in Table 4 are quite large at the last few time steps so the data at the last few time steps in each simulation should be regarded with suspicion.

The length scales for the axisymmetric strain cases are given in Table 5. We were unable to fit these data in the manner applied to the sheared turbulence data. This is probably a result of the maximum total strain in these cases (approximately 2) being much smaller than the total shear in the shear cases (approximately 18); the small total strains are a consequence of the numerical methods used in the full simulations. The initial spectrum of all cases was the same although the initial Reynolds numbers were varied over a factor of two by changing the viscosity, and strain rates were varied over a wide range. If we assume that there is a unique 'equilibrium' spectrum for each turbulence Reynolds number and production/dissipation ratio, the initial conditions cannot be appropriate as each simulation develops, but this does not happen until the total strain is well beyond the limit reached in these simulations. Hence, the strain simulations are somewhat immature and we cannot use them to study the behavior of the length scales.

Despite the difficulties with the strain flows, one can conclude that the length scale based on the dissipation is more appropriate to homogeneous sheared turbulence than is the mixing length, and is likely to apply to a wider range of flows than the mixing length.

4. Test of Models of the Dissipation Equation

4.1 Strategy

In the preceding chapter, we found that, at least for homogeneous shear flow, the length scale based on the dissipation rate is roughly proportional to the length scale associated with the transport of momentum across the mean streamlines. This indicates that the length scale estimate used in many turbulence models is well chosen. However, because the study of the length scales was based on the results of full simulations, we were able to use the exact dissipation in the analysis. In model calculations of turbulent flows, the dissipation is defined by the solution of a partial differential equation. Although an exact equation governing the rate of dissipation of turbulence can be derived, it contains correlations of fluctuating velocity components of order higher than two. These correlations cannot be evaluated and models for them are necessarily uncertain. Consequently, the models used in the dissipation equation are empirical, making them the weakest points in current turbulence models.

For homogeneous turbulent flows, the commonly used model dissipation equation is:

$$\frac{d\epsilon}{dt} = C_{2\epsilon} \frac{\epsilon^2}{k} + C_{1\epsilon} \frac{P\epsilon}{k} \tag{8}$$

where k is the turbulence kinetic energy and P is the rate of production of turbulence kinetic energy given by:

$$P = - \overline{u_i' u_j'} \, S_{ij} \tag{9}$$

where S_{ij} is the strain rate defined by Eq. (2), and $C_{1\epsilon}$ and $C_{2\epsilon}$ are model parameters that are usually treated as constants.

In this chapter, we shall use the full simulation results to evaluate both the validity of this model and the parameters it contains. For this purpose, we need the dissipation and its time derivative. The dissipation is computed in the full simulations and is available; its time derivative is obtained by differentiation. The differentiation was accomplished by spline fitting the dissipation; this method was preferred over finite differencing because the data points are widely spaced. The derivatives obtained in this way contain considerable uncertainty which carries over to the model constants estimated from them. Despite the uncertainty, we should be able to discern trends and thus shed light on a number of important issues connected with modeling the dissipation equation.

For purposes of analyzing the data, it is useful to rewrite Eq. (8) in the form:

$$\frac{k}{\epsilon P} \frac{d\epsilon}{dt} = -C_{2\epsilon} \frac{\epsilon}{P} + C_{1\epsilon} \qquad (10)$$

which suggests that a plot of $(k/\epsilon P)d\epsilon/dt$ and ϵ/P, should be a straight line with slope $C_{2\epsilon}$ and intercept $C_{1\epsilon}$. Such plots provide a stringent test of the model. If the model is valid, the data points will fall on a straight line, and the constants can be extracted by least squares analysis, allowing study of some of the issues raised earlier. We chose to rearrange Eq. (8) so that the data are plotted against ϵ/P rather than P/ϵ, the parameter used by most modelers, because this emphasizes the small P/ϵ data which is more relevant to engineering flows.

In particular, we can compare the parameters obtained from the least squares fit with the generally accepted values. We can also determine whether the same parameter values apply to all homogeneous flows and thus, whether a variety of flows can be fit with a single model. Furthermore, we can determine whether the

constants are independent of the dimensionless variables or
not. As noted earlier, the principal dimensionless variables are
the Reynolds number, $k^2/\varepsilon\nu$, the ratio of production to
dissipation, P/ε, (this is also the ratio of the time scale of
the imposed strain to the turbulence time scale) and the
dimensionless time, St. The tests will occupy the remainder of
this chapter.

4.2 Reduced Data

The quantities necessary for analyzing models of the
dissipation equation were obtained by reducing the data supplied
by Lee and Reynolds (1984) and Rogallo (1981). The production
was calculated in two ways. The first method is essentially
exact; it uses Eq. (9) and the full simulation data for the
Reynolds stresses to compute the rate of turbulence energy
production. This approach takes the model quite literally.

However, in applications, the production is not, and cannot,
be computed this way because the exact Reynolds stresses are not
available. Instead, one must use the model Reynolds stresses
given by Eq. (2). Eq. (9) is then replaced by:

$$P = \frac{8C_\mu k^2}{\varepsilon} S_{ij} S_{ij} \tag{11}$$

Both methods of computing the production will be used.

The proposed tests require the time derivative of the
dissipation. This quantity was obtained by spline fitting the
dissipation as a function of time for each run and
differentiating the result. The wide spacing of the times at
which the data were provided (a consequence of the deforming
grids used in the full simulations) results in large uncertanties
in the computed derivatives. Because they are particularly

-15-

uncertain, the derivatives at the first and last time steps of each run were not used in this analysis. The same values of $d\varepsilon/dt$ were used in both approaches to model testing; this choice was made on the basis of two arguments: 1) these are the only data available for this quantity and 2) an accurate model would yield the correct dissipation, and therefore, the correct time derivative.

The derived data required for the analysis of dissipation models are given in Tables 6-8. Some of the differences between the modeled quantities and the ones obtained from the full simulations are quite large; for the strain flows this is due to a combination of the high strain rates and the short time span of the simulations. It is not surprising that these differences produce significant differences in the results presented below.

4.3 Analysis of the Data

The derived data were used to study the validity of the model represented by Eq. (8). The results for $(k/\varepsilon P)d\varepsilon/dt$ were plotted vs. ε/P for each of the three homogeneous turbulent flows. Least squares straight lines were fit to the data derived from each individual run and to the combined data for each flow. The data points based on the exact production, the least squares fits to those data, and the prediction of the standard model (for which the constants are $C_{1\varepsilon} = 1.44$ and $C_{2\varepsilon} = 1.92$) are shown for each of the three flows in Figures 8-10, respectively. Figures 11-13 give similar results based on the model production given by Eq. (11). The parameters obtained from the least squares fits for each run and the complete data set for each flow are given in Table 9.

A few conclusions can be drawn immediately from these figures. There is considerable scatter in the data and, although straight lines fit the data reasonably well, the resulting parameters contain considerable uncertainty; we cannot estimate this uncertainty accurately but it is probably $\pm.25$ for each parameter. The uncertainty is demonstrated by the fact that the standard model fits the data nearly as well as the least squares lines in Figures 8 and 9, despite significant differences in the parameters. Thus, the parameter values extracted from the full simulation data should not be accepted without allowance for the uncertainty.

The scatter in the data can be attributed to at least three separate sources. The first is the uncertainty in the time derivative of the dissipation; this uncertainty was shown earlier to be a consequence of differentiating data at widely spaced time steps at which the raw data were available. A second source of uncertainty is the relative immaturity of the flows, especially the strain flows. All simulations began with isotropic turbulence as an initial condition; in others, the isotropic turbulence was allowed to develop for some time. Considerable time is required for the flows to display the characteristics of a fully developed strain flow. Unfortunately, the simulations must be stopped when the length scales become too large for the computational region. As a result, the simulations may contain only a small span of developed flow, most of the flow is transitional. A third cause of uncertainty, which may be related to the preceding one, is the tendency of individual runs to follow trajectories that differ considerably from both the least square fits to the full data sets and the standard model. This is reflected by wide scatter among the parameters derived from individual runs and their differences from the values derived from the full data sets. Individual run trajectories are illustrated in Figure 14, which is identical to Figure 8 except for the inclusion of lines representing individual runs; the lines representing the overall fit and the standard model have

been omitted for clarity.

Although the data based on the modeled production show no more scatter than those based on the exact production, the parameters obtained by fitting these data show both wider scatter among themselves and greater deviation from the standard values. This is probably due to the immaturity of the flows and the inability of the model to represent the production well in the early region of highly strained flows. We shall therefore work exclusively with the data derived from the full simulations in the remainder of this report.

From Figures 8 and 9, we see that the standard model fits the data for plane strain and shear reasonably. However, Figure 10 shows that the line representing the standard model lies well outside the data band for axisymmetric strain. Especially, the slope of the standard model line (governed by the parameter $C_{2\varepsilon}$) is too large. The inability of the standard model to fit the data for axisymmetric flows may be related to the difficulty that modelers have had in finding a single model capable of fitting both plane and axisymmetric jets. When models derived for plane flows are applied to axisymmetric flows, the rates of growth of the predicted flows are incorrect. This result argues for caution in applying a single model to a variety of flows; these results are evidence of the need for zonal models. This answers one of the key questions raised at the beginning of this report.

From Figures 8-13 we also note that, although the data scatter considerably about the straight line fits, there is no indication that the relationship between $(k/\varepsilon P)d\varepsilon/dt$ and ε/P is anything other than linear. In other words, there is no reason to expect the parameters to depend on P/ε.

The scatter in the data might be reduced and the fit to the model might be improved by making the model 'constants'—we have called them parameters above and will continue to do so— functions of the nondimensional variables. The argument of the preceding paragraph shows dependence of the parameters on P/ϵ to be improbable. We considered the possibility that the variation in the parameters is due to Reynolds number dependence. However, the Reynolds numbers are large enough that the model parameters should not depend on this parameter. An attempt to fit the parameters for the plane strain case as functions of the Reynolds number produced an irregular and stronger than expected functional dependence, so the possibility of Reynolds number dependence of the parameters was rejected. The remaining possibility is that the parameters are functions of the nondimensional time St. We shall explore this next.

To test the possibility that the model parameters are functions of the total strain, St, we sorted the data from the various runs (Tables 6-8) according to the value of the total strain. For each total strain, a least squares fit to the data was made; the results are presented in Table 10. In this process, some of the data were not used because there were not enough data for all values of the total strain. For this reason, the overall values presented in Table 10 may differ from those in Table 9. The data for the plane strain cases showing the lines of constant total strain are plotted in Figure 15; the data for different total strains clearly fall on lines of different slope but the same intercept indicating that, for this flow at least, $C_{1\epsilon}$ may be taken as constant but $C_{2\epsilon}$ is a function of St. This conclusion is borne out by the least squares parameters for this flow presented in Table 10.

The results for the shear flow cases are shown in Figure 16. For this flow, there is no indication that the data for different St require different values of the parameters. Indeed, the derived parameters given in Table 10 show considerable scatter and no discernable trend. On closer examination, one sees that the data for each St cover a very narrow range of P/ε , indicating that the production develops more quickly in the shear flow than in the strain flows; this characteristic has been noted by others (eg., Tzuoo et al, 1984). For sheared turbulence, the parameters can be regarded as constants.

For the axisymmetric strain flow cases, the lines of constant St are shown in Figure 17. Notice that the overall fit is especially influenced by the data for the smallest value of St, the data set with the largest ratio of dissipation to production (see Table 8). Since this data set represents the least mature flows, we decided to eliminate it from the overall analysis and redo the overall fit. The result is shown in Fig. 18; the constants are given in Table 10. We see that, in contrast to the case of sheared turbulence, the data can be fit with the standard value of $C_{2\varepsilon}$, but the value of $C_{1\varepsilon}$ needs to be changed to fit these data.

To sum up, we find that a single model of the dissipation equation cannot fit the data for a variety of different kinds of strain. For turbulence undergoing plane strain, dependence of the parameter $C_{2\varepsilon}$ on the total strain St is required. On the other hand, the sheared turbulence data can be fit with constant parameters; the standard parameters do well in this case. Finally, for turbulence undergoing axisymmetric strain, constant parameters appear to suffice but a value of the parameter $C_{1\varepsilon}$ larger than the total strain is small in both strain cases; the resulting parameters may be inaccurate for these cases.

5. Conclusions

We have investigated a number of issues connected with
turbulence and its modeling by using the results of full
simulations of homogeneous turbulent flows as the database. One
of the principal conclusions reached in this study is that it is
indeed possible to use full turbulence simulation results (and,
presumably, large eddy simulation results as well) to study both
the physics of turbulence and turbulence modeling. A principal
recommendation resulting from this study is that such simulations
be used when feasible for the purposes to which they have been
put in this study; combination of simulation data with
experimental data would be even more desirable. The development
of new methods of investigating the data would be valuable and is
therefore highly recommended.

Turning to specific conclusions to be drawn from this study,
we have shown that, the mechanism of turbulence production in
homogeneous sheared turbulence resembles the mechanism of the
near-wall part of a boundary layer more than the mechanism of the
turbulence production in the mixing layer. Despite this, the
standard model dissipation equation that is often used for
inhomogeneous shear flows works well in the homogenous flow. It
thus appears that it is possible to fit a wide range of shear
flows, which have greatly different physical behavior, with a
single turbulence model. We do not understand the reason why
this is so, but it is very encouraging.

The length scale based on the dissipation that is commonly
used to model the integral scale works quite well for homogeneous
shear flow. However, an adjustment to the usual formula needs to
be made at low Reynolds numbers. The mixing length fits the
integral scale well only over a narrow range of the ratio of
production to dissipation and should be used only for
'equilibrium' flows which meet this criterion. For the strain

-21-

flows, the limited range of total strain for which data were available made it impossible to study the behavior of the length scales in a satisfactory manner.

We found that the model parameters need to be different for each class of flow. In particular, the standard model is satisfactory for sheared turbulence but not the strain flows. For the case of plane strain, it appears to be necessary to make the parameter $C_{2\epsilon}$ of the modeled dissipation equation a function of the total strain. On the other hand, the axisymmetric strain cases require a change in the parameter $C_{1\epsilon}$; a constant value appears to be satisfactory. The limited range of total strain that we were able to study suggests that this portion of the work be repeated when data covering a broader range of total strain become available.

ACKNOWLEDGEMENTS

REFERENCES

Brown G. L. and Roshko, A. (1974): On Density Effects and Large Structure in Turbulent Mixing Layers, J. Fluid Mech., Vol. 64, p. 775.

Cain, A. B., Reynolds, W. C., and Ferziger, J. H. (1981): A Three Dimensional Simulation of Transition and Early Turbulence in a Time Developing Mixing Layer, Report TF-14, Dept. of Mech. Engr., Stanford University.

Chandrsuda, C., Mehta, R. D., Weir, A. D., and Bradshaw, P. (1978): Effect of Free-Stream Turbulence on Large Structure in Turbulent Mixing Layers, J. Fluid Mechanics., Vol. 85, pp. 693-704.

Corcos, G. M. and Lin, S. J. (1984): The Mixing Layer: Deterministic Models of a Turbulent Flow. Part 2. The Origin of the Three-Dimensional Motion, J. Fluid Mech., Vol. 139, pp. 67-95.

Feiereisen, W. J., Reynolds, W. C., and Ferziger, J. H. (1981): Simulation of Compressible Homogeneous Turbulent Flows and their Application to Turbulence Modeling, Report TF-13, Dept. of Mech. Engr., Stanford University.

Kline, S. J., Reynolds, P., Schraub, F. A., and Runstadler, P. W. (1967): The Structure of Turbulent Boundary Layers, J. Fluid Mech., Vol. 30, pp. 741-773.

Konrad, J. H. (1976): An Experimental Investigation of Mixing in Two-Dimensional Turbulent Shear Flow with Application to Diffusion Limited Chemical Reactions. Rept. CIT-8-PU, Cal. Inst. Tech.

Lee, M. J. and Reynolds, W. C., to be published.

Moore, D. W. and Saffman, P. G. (1975): The Density of Organized Vortices in a Turbulent Mixing Layer, J. Fluid Mech., Vol. 69, pp. 465-473.

Pierrehumbert R. T., and Widnall, S. E. (1982): The Two-and Three-Dimensional instabilities of a Spatially Periodic Shear Layer, J. Fluid Mech., Vol. 114, pp. 59-82.

Rogallo, R. S. (1981): Numerical Experiments in Homogeneous Turbulence, NASA Tech. Memo 81315.

Rogers, M. and Moin, P., to be published.

REFERENCES (concluded)

Shirani, E., Ferziger, J. H., and Reynolds, W. C. (1981):
Simulation of Homogeneous Shear Flow Containing a Passive
Scalar, Report TF-15, Dept. of Mech. Engr., Stanford
University.

Tennekes and Lumley (1982): A First Course in Turbulence,
Cambridge, Mass. MIT Press.

Winant, C. D. and Browand, F. K. (1974): Vortex Pairing:
The Mechanism of Mixing Layer Growth at Moderate Reynolds
Number, J. Fluid Mech., Vol. 63, p. 237.

Table 1

Data for Homogeneous Turbulence Undergoing Plane Strain
From Lee and Reynolds (1984)

Time	Kinetic Energy	Dissipation	Turbulence Components		
T	q^2	ε	U_1^2	U_2^2	U_3^2
S = 0.65					
0.0000	0.1304	0.0847	0.0441	0.0424	0.0439
0.5385	0.0771	0.0354	0.0263	0.0326	0.0182
1.0710	0.0610	0.0208	0.0205	0.0309	0.0097
1.6019	0.0586	0.0156	0.0192	0.0330	0.0064
2.1329	0.0639	0.0138	0.0205	0.0386	0.0048
S = 1.3					
0.0000	0.1304	0.0847	0.0441	0.0424	0.0439
0.2700	0.1002	0.0558	0.0346	0.0418	0.0238
0.5366	0.0911	0.0438	0.0318	0.0450	0.0143
0.8033	0.0944	0.0389	0.0328	0.0518	0.0098
1.0670	0.1074	0.0383	0.0371	0.0630	0.0074
S = 2.6					
0.0000	0.1304	0.0847	0.0441	0.0424	0.0439
0.1366	0.1165	0.0729	0.0406	0.0483	0.0276
0.2685	0.1177	0.0725	0.0426	0.0567	0.0184
0.4009	0.1304	0.0770	0.0482	0.0692	0.0130
0.5309	0.1542	0.0853	0.0574	0.0870	0.0097
S = 5.2					
0.0000	0.1304	0.0847	0.0441	0.0424	0.0439
0.0683	0.1266	0.0847	0.0443	0.0522	0.0301
0.1354	0.1372	0.1001	0.0510	0.0649	0.0213
0.2013	0.1602	0.1242	0.0623	0.0824	0.0155
0.2670	0.1970	0.1558	0.0782	0.1072	0.0116
S = 25					
0.0000	0.1304	0.0847	0.0441	0.0424	0.0439
0.0155	0.1370	0.0985	0.0485	0.0570	0.0315
0.0285	0.1581	0.1382	0.0605	0.0734	0.0242
0.0418	0.1953	0.2133	0.0804	0.0963	0.0186
0.0558	0.2554	0.3423	0.1106	0.1308	0.0140
S = 100					
0.0000	0.1304	0.0847	0.0441	0.0424	0.0439
0.0034	0.1368	0.0970	0.0480	0.0555	0.0333
0.0078	0.1704	0.1646	0.0669	0.0799	0.0236
0.0112	0.2169	0.2787	0.0920	0.1065	0.0183
0.0136	0.2637	0.4145	0.1166	0.1319	0.0153

Table 2
Data for Homogeneous Shear Flow
From Rogallo (1981)

Time	Kinetic Energy	Dissipation	Reynolds Shear Stress
t	k	ϵ	$\overline{u_2'u_2'}/q^2$
Case BSH9	$S = 28.28$		
0.0707	8.2459	130.8352	-0.1544
0.1414	6.2240	64.8076	-0.1693
0.2121	6.5075	48.8456	-0.1675
0.2828	7.7987	48.2009	-0.1648
0.3536	9.8547	55.4535	-0.1603
0.4243	12.5860	69.1574	-0.1594
0.4950	16.0822	87.8498	-0.1602
0.5657	20.6653	112.7094	-0.1563
0.6364	25.7101	146.5232	-0.1522
Case BSH10	$S = 28.28$		
0.0707	5.1572	95.1088	-0.1731
0.1414	3.9861	42.6498	-0.1785
0.2121	4.1558	33.6941	-0.1674
0.2828	4.7527	32.0710	-0.1612
0.3536	5.7482	33.6144	-0.1557
0.4243	7.2030	38.2974	-0.1541
0.4950	9.3365	45.0482	-0.1550
Case BSH11	$S = 56.56$		
0.0354	11.2136	261.3250	-0.1788
0.0707	11.4356	198.7566	-0.1818
0.1061	13.1627	187.9649	-0.1679
0.1414	15.7866	197.7942	-0.1614
0.1768	19.8112	221.9700	-0.1624
0.2121	25.9920	265.9385	-0.1607
0.2475	34.7631	337.6216	-0.1613
Case BSH12	$S = 20$		
0.1000	9.1089	61.3060	-0.1498
0.2000	8.5069	55.6731	-0.1586
0.3000	8.7937	47.5697	-0.1593
0.4000	9.9933	46.5868	-0.1595
0.5000	12.0217	49.3771	-0.1564
0.6000	14.7169	60.0536	-0.1512

Table 3
Data for Homogeneous Turbulence Undergoing Axisymmetric
Strain From Rogallo (1981)

Time	Kinetic Energy	Dissipation	Reynolds Stress Anisotropy	
T	q^2	E	B11	B22=B33
S = 10				
0.0236	4.3901	64.3063	-0.0510	0.0255
0.0468	3.3578	45.2619	-0.1146	0.0573
0.0700	2.7549	33.3630	-0.1666	0.0833
0.0941	2.4018	25.4876	-0.2068	0.1034
0.1160	2.2306	21.0812	-0.2333	0.1166
0.1387	2.1476	18.4767	-0.2538	0.1269
S = 20				
0.0125	5.1941	80.0632	-0.0550	0.0275
0.0241	4.6231	71.1713	-0.1202	0.0601
0.0359	4.2818	66.4785	-0.1752	0.0876
0.0462	4.1166	63.9339	-0.2118	0.1059
0.0586	4.0338	61.6251	-0.2442	0.1221
0.0698	4.0462	60.1506	-0.2654	0.1327
S = 40				
0.0061	5.7336	90.6299	-0.0527	0.0263
0.0120	5.5530	91.1385	-0.1219	0.0610
0.0185	5.6178	100.2140	-0.1859	0.0929
0.0236	5.8010	111.7112	-0.2239	0.1120
0.0293	6.1111	128.1692	-0.2560	0.1280
0.0352	6.4979	146.3656	-0.2786	0.1393
S = 5				
0.0466	3.2022	41.7351	-0.0503	0.0251
0.0929	1.9867	20.1809	-0.1145	0.0573
0.1397	1.4483	11.2151	-0.1659	0.0829
0.1866	1.1944	7.3673	-0.2020	0.1010
0.2332	1.0658	5.6087	-0.2275	0.1138
0.2791	0.9988	4.7363	-0.2467	0.1233
S = 10				
0.0233	2.7378	43.1753	-0.0643	0.0321
0.0481	2.0563	27.7339	-0.1354	0.0677
0.0695	1.7366	20.7865	-0.1833	0.0916
0.0940	1.5279	16.5394	-0.2224	0.1112
0.1170	1.4130	14.4098	-0.2485	0.1243
0.1387	1.3455	13.2673	-0.2671	0.1335

Table 3 concluded

S = 20

0.0120	3.2893	56.9968	-0.0651	0.0326
0.0240	2.8856	48.2453	-0.1349	0.0675
0.0359	2.6675	43.4551	-0.1912	0.0956
0.0477	2.5635	41.0395	-0.2323	0.1162
0.0586	2.5316	40.3360	-0.2592	0.1296
0.0696	2.5371	40.7194	-0.2788	0.1394

S = 40

0.0065	3.6322	66.2693	-0.0705	0.0352
0.0131	3.5055	66.6514	-0.1464	0.0732
0.0185	3.5308	70.9752	-0.1984	0.0992
0.0236	3.6329	77.4141	-0.2364	0.1182
0.0296	3.8222	86.9958	-0.2686	0.1343
0.0349	4.0319	96.9658	-0.2881	0.1441

S = 5

0.0475	1.9472	25.4329	-0.0681	0.0340
0.0925	1.2536	12.3167	-0.1313	0.0657
0.1406	0.9224	7.2250	-0.1808	0.0904
0.1865	0.7585	5.1039	-0.2139	0.1069
0.2326	0.6618	4.0033	-0.2384	0.1192
0.2774	0.6023	3.3940	-0.2573	0.1287

Table 4

Length Scales in Sheared Turbulence

Time	Reynolds Number	Mixing Length	Integral Scale $L_{11,2}$	Dissipation Length
Case BSH9				
0.0707	73.50	0.0564	0.0799	0.5119
0.1414	84.53	0.0513	0.1067	0.6777
0.2121	122.61	0.0522	0.1260	0.9613
0.2828	178.45	0.0567	0.1537	1.2780
0.3536	247.67	0.0628	0.1549	1.5779
0.4243	323.93	0.0708	0.1784	1.8262
0.4950	416.36	0.0802	0.1584	2.0765
0.5657	535.85	0.0899	0.2277	2.3575
0.6364	638.00	0.0989	0.2665	2.5165
Case BSH10				
0.0707	19.77	0.0472	0.0981	0.3483
0.1414	26.34	0.0422	0.1195	0.5278
0.2121	36.24	0.0417	0.1487	0.7112
0.2828	49.80	0.0438	0.1638	0.9138
0.3536	69.51	0.0473	0.1535	1.1596
0.4243	95.79	0.0527	0.1841	1.4277
0.4950	136.83	0.0601	0.2210	1.7912
Case BSH11				
0.0354	34.02	0.0708	0.0635	0.4064
0.0707	46.52	0.0721	0.0575	0.5503
0.1061	65.18	0.0743	0.1182	0.7186
0.1414	89.09	0.0798	0.1347	0.8969
0.1768	125.03	0.0897	0.1297	1.1236
0.2121	179.63	0.1022	0.1489	1.4094
0.2475	253.10	0.1184	0.1516	1.7171
Case BSH12				
0.1000	270.68	0.0584	0.1124	1.2683
0.2000	259.97	0.0581	0.1485	1.2605
0.3000	325.12	0.0592	0.1643	1.5505
0.4000	428.73	0.0631	0.2264	1.9180
0.5000	585.38	0.0686	0.2833	2.3876
0.6000	721.32	0.0746	0.2687	2.6591

Table 5

Length Scales in Axisymmetric Strained Turbulence

Total Strain	Reynolds Number	Mixing Lengths 1	2	Integral Scales 11,1	22,2	Mean	Dissipation Length
Case CD11	**S = 10**						
0.2363	42.38	0.1113	0.2510	0.1068	0.1122	0.1913	0.1430
0.4684	35.23	0.0857	0.2291	0.1018	0.1222	0.2006	0.1359
0.7002	32.17	0.0678	0.2143	0.0931	0.1317	0.2082	0.1371
0.9407	32.01	0.0551	0.2048	0.0819	0.1392	0.2132	0.1460
1.1599	33.38	0.0472	0.2004	0.0730	0.1432	0.2153	0.1580
1.3870	35.30	0.0413	0.1988	0.0666	0.1427	0.2125	0.1703
Case CD12	**S = 20**						
0.2499	47.66	0.0601	0.1369	0.1047	0.1074	0.1845	0.1479
0.4816	42.47	0.0496	0.1349	0.0993	0.1105	0.1852	0.1397
0.7182	39.00	0.0411	0.1343	0.0912	0.1124	0.1833	0.1333
0.9243	37.48	0.0354	0.1345	0.0824	0.1136	0.1806	0.1306
1.1715	37.34	0.0300	0.1355	0.0717	0.1142	0.1767	0.1315
1.3953	38.49	0.0262	0.1373	0.0636	0.1135	0.1727	0.1353
Case CD13	**S = 40**						
0.2426	51.30	0.0317	0.0718	0.1040	0.1048	0.1811	0.1515
0.4817	47.85	0.0271	0.0740	0.1001	0.1044	0.1784	0.1436
0.7413	44.54	0.0228	0.0774	0.0941	0.1018	0.1720	0.1329
0.9429	42.60	0.0199	0.0804	0.0880	0.0992	0.1656	0.1251
1.1739	41.21	0.0172	0.0840	0.0802	0.0963	0.1580	0.1179
1.4066	40.80	0.0149	0.0876	0.0736	0.0924	0.1500	0.1132
Case CD14	**S = 5**						
0.2330	34.75	0.1904	0.4286	0.1122	0.1224	0.2063	0.1373
0.4643	27.66	0.1319	0.3524	0.1113	0.1457	0.2342	0.1388
0.6983	26.45	0.0985	0.3106	0.1046	0.1635	0.2538	0.1554
0.9328	27.39	0.0792	0.2881	0.0955	0.1718	0.2611	0.1772
1.1662	28.64	0.0672	0.2761	0.0950	0.1762	0.2667	0.1962
1.3955	29.79	0.0588	0.2701	0.0766	0.1782	0.2634	0.2107
Case CD21	**S = 10**						
0.2326	12.28	0.0858	0.2001	0.1366	0.1465	0.2482	0.1049
0.4805	10.78	0.0638	0.1816	0.1362	0.1625	0.2671	0.1063
0.6953	10.26	0.0510	0.1718	0.1259	0.1714	0.2731	0.1101
0.9404	9.98	0.0412	0.1648	0.1093	0.1793	0.2761	0.1142
1.1705	9.80	0.0396	0.1608	0.0941	0.1826	0.2798	0.1166
1.3866	9.65	0.0299	0.1585	0.0835	0.1835	0.2726	0.1176

Table 5. Concluded

Case CD22   S = 20

0.2402	13.42	0.0470	0.1097	0.1316	0.1380	0.2354	0.1047
0.4796	12.20	0.0378	0.1075	0.1297	0.1435	0.2408	0.1016
0.7171	11.58	0.0308	0.1070	0.1237	0.1476	0.2426	0.1003
0.9550	11.32	0.0254	0.1073	0.1134	0.1456	0.2351	0.1000
1.1720	11.24	0.0217	0.1083	0.1018	0.1493	0.2344	0.0999
1.3911	11.18	0.0186	0.1095	0.0907	0.1481	0.2282	0.0992

Case CD23   S = 40

0.2605	14.08	0.0244	0.0579	0.1290	0.1336	0.2288	0.1045
0.5223	13.04	0.0202	0.0597	0.1272	0.1334	0.2275	0.0985
0.7384	12.42	0.0173	0.0618	0.1244	0.1315	0.2237	0.0935
0.9431	12.06	0.0148	0.0640	0.1202	0.1289	0.2184	0.0894
1.1843	11.87	0.0124	0.0668	0.1136	0.1254	0.2106	0.0859
1.3959	11.85	0.0107	0.0694	0.1069	0.1222	0.2032	0.0835

Case CD24   S = 5

0.2373	10.54	0.1437	0.3383	0.1469	0.1637	0.2742	0.1068
0.4623	9.02	0.1006	0.2829	0.1458	0.1896	0.3052	0.1140
0.7031	8.33	0.0750	0.2501	0.1311	0.2080	0.3220	0.1226
0.9327	7.97	0.0602	0.2312	0.1144	0.2194	0.3307	0.1294
1.1631	7.74	0.0501	0.2189	0.1021	0.2265	0.3362	0.1345
1.3872	7.56	0.0428	0.2110	0.0955	0.2306	0.3398	0.1377

Table 6
Derived Data--Plane Strain

Time T	$d\epsilon/dt$	Prod.	Exact quantities ϵ/p	$(k/\epsilon P)d\epsilon/dt$	Model quantites Prod.	$(k/\epsilon P)de/dt$	
	S = .65						
0.538	-0.04170	0.009	3.785	-4.868	0.026	1.383	-1.778
1.071	-0.01308	0.014	1.514	-1.393	0.027	0.766	-0.705
1.602	-0.00674	0.017	0.900	-0.734	0.034	0.464	-0.378
	S = 1.3						
0.270	-0.06303	0.023	2.381	-2.415	0.109	0.510	-0.517
0.537	-0.02643	0.040	1.099	-0.691	0.115	0.379	-0.238
0.803	-0.00997	0.055	0.713	-0.222	0.139	0.279	-0.087
	S = 2.6						
0.137	-0.02663	0.054	1.360	-0.397	0.453	0.161	-0.047
0.269	0.019325	0.099	0.729	0.158	0.465	0.156	0.034
0.401	0.048409	0.146	0.527	0.281	0.538	0.143	0.076
	S = 5.2						
0.068	0.150536	0.115	0.739	0.981	1.842	0.046	0.061
0.135	0.308486	0.227	0.441	0.932	1.831	0.055	0.115
0.201	0.422935	0.348	0.357	0.784	2.012	0.062	0.136
	S = 25						
0.015	1.899254	0.637	0.155	2.074	42.883	0.002	0.031
0.028	4.046675	1.229	0.112	1.884	40.700	0.003	0.057
0.042	7.270794	1.943	0.110	1.713	40.226	0.005	0.083
	S = 100						
0.003	6.246672	2.214	0.044	1.990	694.221	.000	0.006
0.008	21.51598	5.623	0.029	1.980	634.706	.000	0.018
0.011	46.55979	8.820	0.032	2.054	607.615	.000	0.030

Table 7

Derived Data--Sheared Turbulence

Time,t	$d\epsilon/dt$	Prod.	Exact Quantities ϵ/P	$(k/\epsilon P)d\epsilon/dt$	Model Quantities Prod.	ϵ/P	$(k/\epsilon P)d\epsilon/dt$
			$S = 28.28$				
0.141	-517.5	59.60	1.087	-0.834	86.08	0.753	-0.577
0.212	-58.3	61.65	0.792	-0.126	124.84	0.391	-0.062
0.283	46.4	72.70	0.663	0.103	181.70	0.265	0.041
0.354	153.2	89.37	0.621	0.305	252.19	0.220	0.108
0.424	229.8	113.50	0.609	0.369	329.84	0.210	0.127
0.495	301.9	145.71	0.603	0.379	423.95	0.207	0.130
0.566	410.3	182.74	0.617	0.412	545.62	0.207	0.138
			$S = 28.28$				
0.141	-367.9	40.25	1.060	-0.854	53.65	0.795	-0.641
0.212	-18.2	39.36	0.856	-0.057	73.81	0.457	-0.030
0.283	-8.2	43.33	0.740	-0.028	101.42	0.316	-0.012
0.354	47.5	50.63	0.664	0.161	141.55	0.237	0.057
0.424	82.2	62.80	0.610	0.246	195.08	0.196	0.079
			$S = 56.56$				
0.071	-926.7	235.15	0.845	-0.227	378.98	0.524	-0.141
0.106	94.7	250.00	0.752	0.027	530.93	0.354	0.012
0.141	466.1	288.27	0.686	0.129	725.75	0.273	0.051
0.177	926.4	364.07	0.610	0.227	1018.47	0.218	0.081
0.212	1610.7	472.56	0.563	0.333	1463.26	0.182	0.108
			$S = 20$				
0.200	-83.1	53.96	1.032	-0.235	93.59	0.595	-0.136
0.300	-50.2	56.02	0.849	-0.166	117.04	0.406	-0.079
0.400	11.2	63.75	0.731	0.038	154.34	0.302	0.016
0.500	75.4	75.20	0.657	0.244	210.74	0.234	0.087

Table 8

Derived Data-- Axisymmetric Strain

Time,t	$d\epsilon/dt$	Prod.	Exact Quantites ϵ/P	$(k/\epsilon P)d\epsilon/dt$	Model Quantities Prod.	ϵ/P	$(k/\epsilon P)d\epsilon/dt$
S = 10							
0.024	-989.60	3.357	19.159	-20.128	8.092	7.947	-8.349
0.047	-651.98	5.774	7.840	-8.378	6.726	6.729	-7.191
0.070	-404.49	6.883	4.847	-4.852	6.142	5.432	-5.438
0.094	-255.05	7.449	3.422	-3.227	6.111	4.171	-3.933
0.116	-154.72	7.806	2.701	-2.097	6.373	3.308	-2.569
0.139	-74.61	8.176	2.260	-1.061	6.740	2.741	-1.287
S = 20							
0.012	-977.06	8.567	9.346	-7.399	36.393	2.200	-1.742
0.024	-558.03	16.666	4.270	-2.175	32.433	2.194	-1.118
0.036	-287.58	22.503	2.954	-0.823	29.785	2.232	-0.622
0.046	-215.12	26.161	2.444	-0.529	28.626	2.233	-0.484
0.059	-158.06	29.553	2.085	-0.350	28.517	2.161	-0.363
0.070	-105.39	32.215	1.867	-0.220	29.395	2.046	-0.241
S = 40							
0.006	-587.15	18.124	5.000	-2.049	156.698	0.578	-0.237
0.012	757.47	40.167	2.244	1.136	146.165	0.624	0.316
0.019	1947.40	62.647	1.600	1.743	136.047	0.737	0.802
0.024	2594.90	77.945	1.433	1.729	130.137	0.858	1.035
0.029	3027.70	93.873	1.365	1.538	125.875	1.018	1.147
0.035	3228.70	108.635	1.347	1.319	124.621	1.174	1.150
S = 5							
0.047	-622.70	1.208	34.549	-39.551	1.658	25.166	-28.809
0.093	-309.51	1.707	11.825	-17.854	1.320	15.286	-23.080
0.140	-114.13	1.802	6.225	-8.181	1.262	8.884	-11.675
0.187	-54.80	1.809	4.072	-4.910	1.307	5.636	-6.797
0.233	-25.70	1.819	3.084	-2.686	1.367	4.103	-3.573
0.279	-12.36	1.848	2.563	-1.410	1.422	3.332	-1.833
S = 10							
0.023	-800.14	2.640	16.355	-19.220	4.688	9.211	-10.824
0.048	-445.70	4.178	6.639	-7.910	4.116	6.737	-8.028
0.070	-232.35	4.774	4.354	-4.066	3.917	5.307	-4.956
0.094	-123.54	5.097	3.245	-2.239	3.811	4.340	-2.995
0.117	-68.63	5.267	2.736	-1.278	3.741	3.852	-1.799
0.139	-37.15	5.390	2.462	-0.699	3.684	3.601	-1.023

Table 8 Concluded

S = 20

0.012	-910.80	6.426	8.869	-8.179	20.501	2.780	-2.564
0.024	-551.28	11.682	4.130	-2.822	18.640	2.588	-1.769
0.036	-285.76	15.298	2.841	-1.147	17.685	2.457	-0.992
0.048	-124.98	17.869	2.297	-0.437	17.294	2.373	-0.451
0.059	-11.71	19.683	2.049	-0.037	17.160	2.351	-0.043
0.070	81.65	21.218	1.919	0.240	17.073	2.385	0.298

S = 40

0.007	-371.68	15.354	4.316	-1.327	86.002	0.771	-0.237
0.013	488.41	30.794	2.164	0.834	79.647	0.837	0.323
0.018	1069.00	42.032	1.689	1.265	75.878	0.935	0.701
0.024	1424.90	51.527	1.502	1.298	73.649	1.051	0.908
0.030	1748.00	61.601	1.412	1.247	72.547	1.199	1.059
0.035	2020.60	69.705	1.391	1.205	72.426	1.339	1.160

S = 5

0.047	-397.29	0.994	25.578	-30.590	1.006	25.274	-30.277
0.092	-185.72	1.235	9.977	-15.312	0.861	14.302	-21.949
0.141	-58.96	1.251	5.777	-6.019	0.795	9.089	-9.469
0.187	-33.52	1.217	4.195	-4.095	0.761	6.708	-6.547
0.233	-17.22	1.183	3.383	-2.405	0.738	5.421	-3.855
0.277	-9.97	1.162	2.920	-1.522	0.721	4.705	-2.452

Table 9
Derived Model Constants

| Strain Rate | Model Constants based on: | | | |
| | Actual Production | | Model Production | |
S	$C_{1\epsilon}$	$C_{2\epsilon}$	$C_{1\epsilon}$	$C_{2\epsilon}$
Plane Strain				
0.65	0.683	1.459	0.400	1.555
1.30	0.740	1.323	0.451	1.880
2.60	0.737	0.830	0.981	6.258
5.20	0.681	-0.426	-0.155	-4.799
25.00	1.074	-6.500	-0.005	-16.854
100.00	2.053	1.301	-0.003	-72.355
Overall	1.768	1.844	0.137	1.261
Sheared Turbulence				
20.00	0.970	1.224	0.204	0.603
28.28	1.874	2.506	0.399	1.281
28.28	1.735	2.343	0.368	1.192
56.56	1.399	1.883	0.243	0.711
Overall	1.580	2.093	0.354	1.099
Axisymmetric Strain				
5.00	-0.290	1.169	0.575	1.269
5.00	1.052	1.278	2.746	1.389
10.00	0.765	1.102	1.938	1.332
10.00	1.953	1.317	4.765	1.762
20.00	1.825	0.977	6.365	3.272
20.0	2.341	1.196	14.528	6.206
40.00	3.083	1.007	-1.008	-2.056
40.00	2.634	0.904	-1.587	-2.191
Overall	2.276	1.277	2.101	1.352
Standard Model				
	1.92	1.44		

Table 10
Derived Model Constants
Based on Actual Production

Total Strain	Model Constants $C_{1\epsilon}$	$C_{2\epsilon}$
Plane Strain		
0.35	2.234	1.896
0.70	2.024	2.362
1.05	2.052	3.196
Overall	1.768	1.844
Sheared Turbulence		
4.00	1.791	2.314
6.00	0.769	1.046
8.00	1.757	2.394
10.00	0.633	0.657
12.00	3.200	4.745
Overall	1.526	2.034
Axisymmetric Strain		
0.24	3.856	1.293
0.48	5.660	1.991
0.71	4.785	1.993
0.94	4.844	2.263
1.17	4.235	2.123
1.39	3.710	1.902
Overall		
All cases	2.276	1.276
Last 5 cases	3.867	1.817
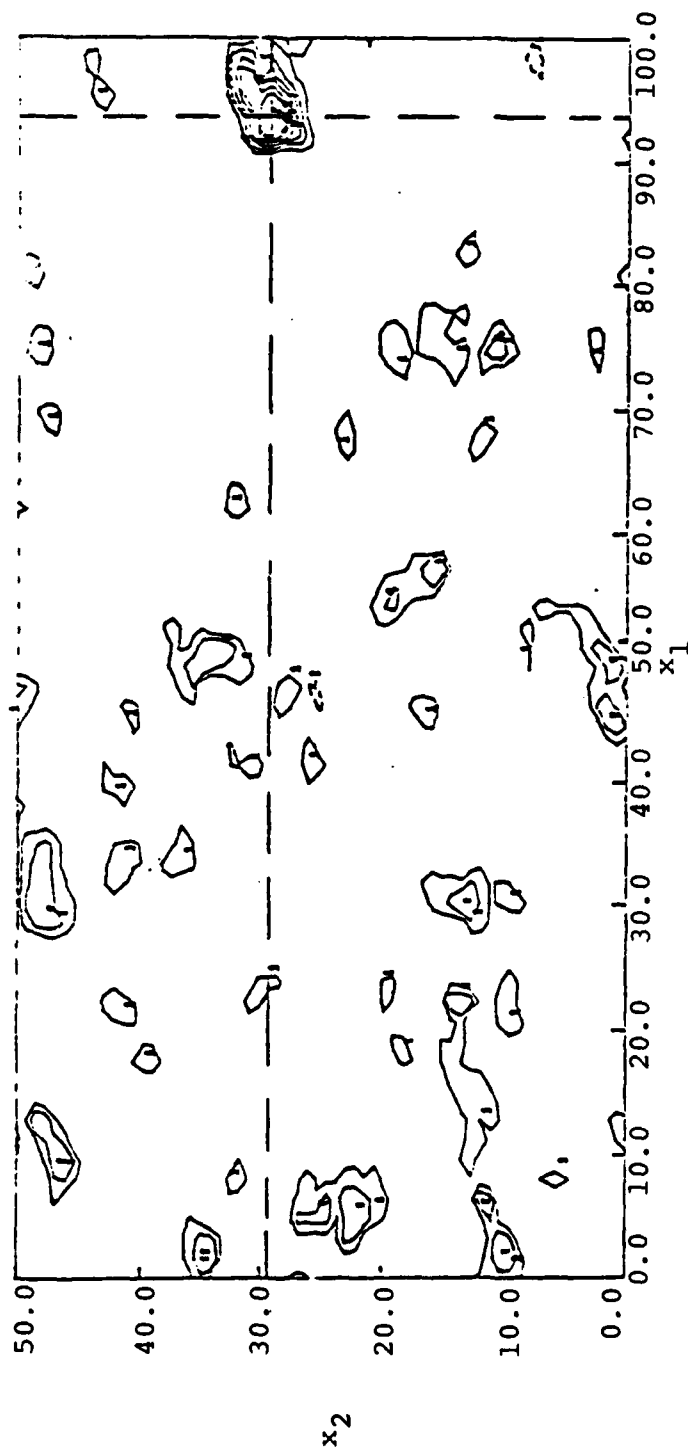
Figure 1. Contour plot in the x_1-x_2 plane of the instantaneous Reynolds stress $u_1 u_2$ in homogeneous shear flow at $St = 14$. The mean flow is in the x_1-direction; its gradient is in the x_2-direction. Note the concentrated region of Reynolds stress on the right side of the figure.
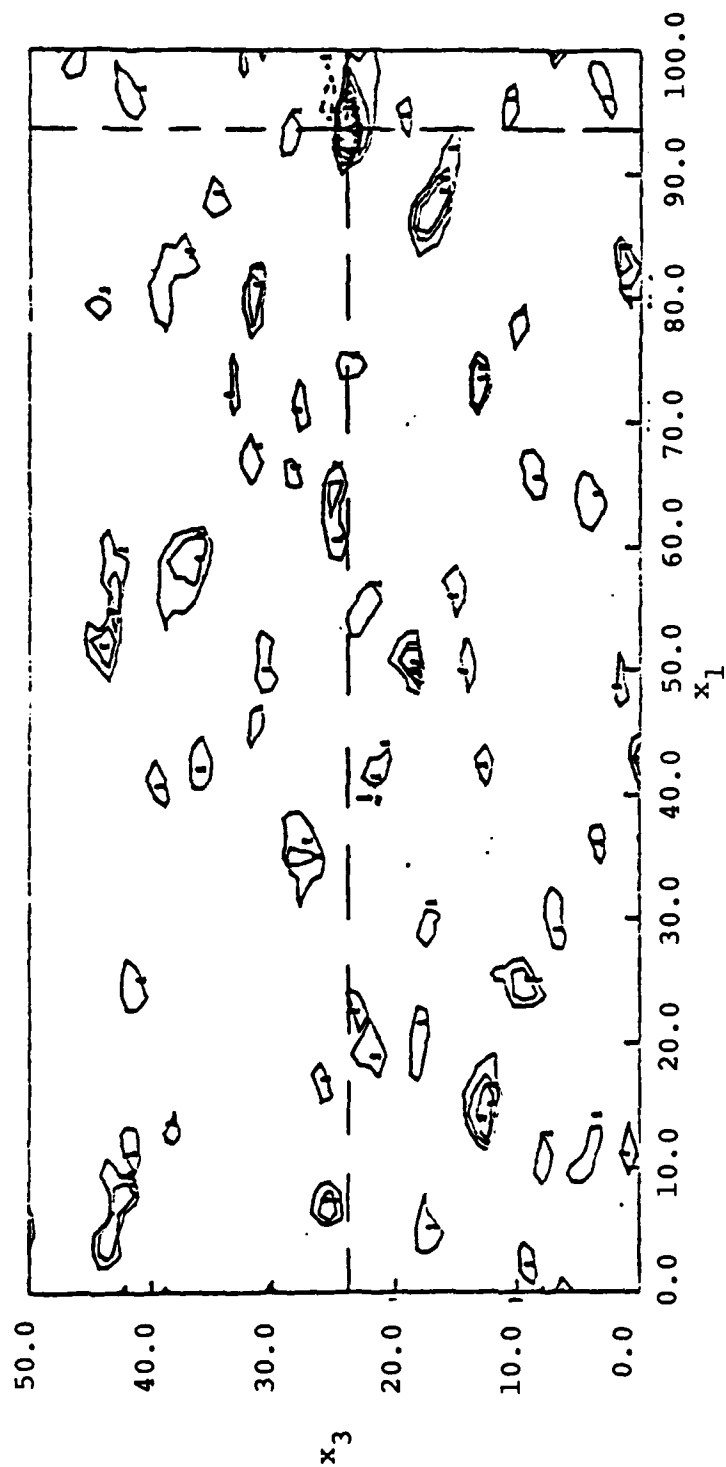
Figure 2. Contour plot of the Reynolds stress in the x_1-x_3 plane; the flow is identical to the one shown in Figure 1. The Reynolds stress concentration on right side marked by the grid lines is the one seen in Figure 1.

-39-
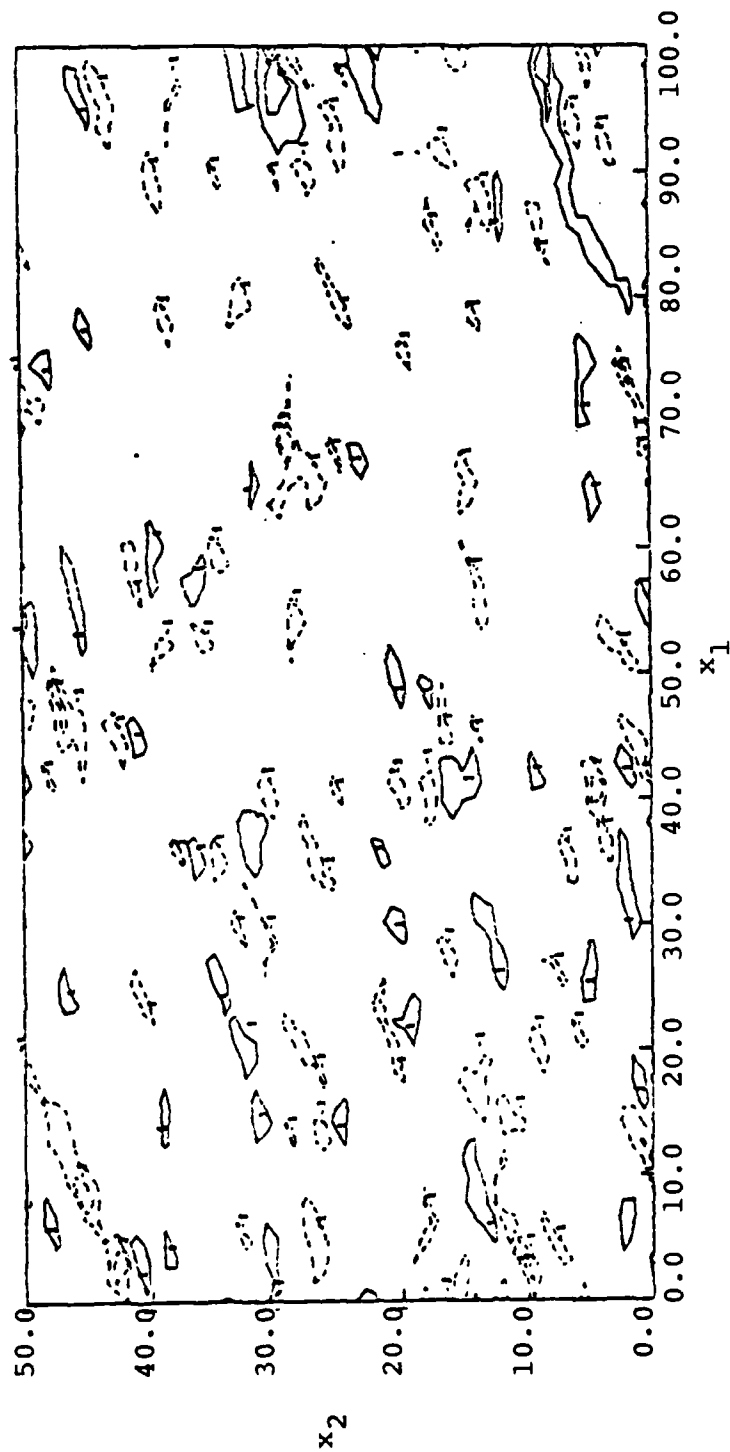
Figure 3. Contours of the streamwise vorticity in the x_1-x_2 plane for the flow shown in Figures 1 and 2. The plane shown in this figure is parallel to the one shown in Figure 1 but displaced by one grid in the spanwise direction.
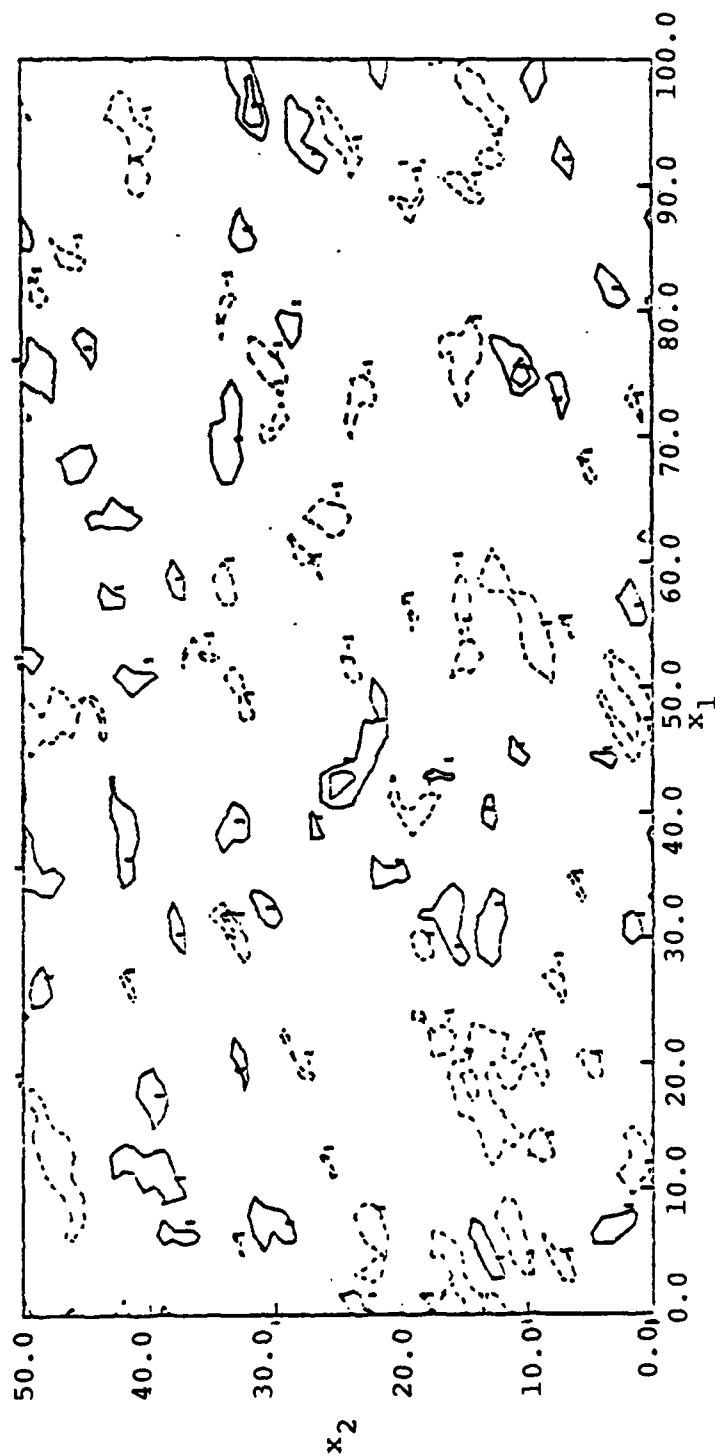
Figure 4. Contours of the vertical vorticity in the x_1-x_2 plane for the flow shown in Figures 1-3. The plane is the one shown in Figure 3.
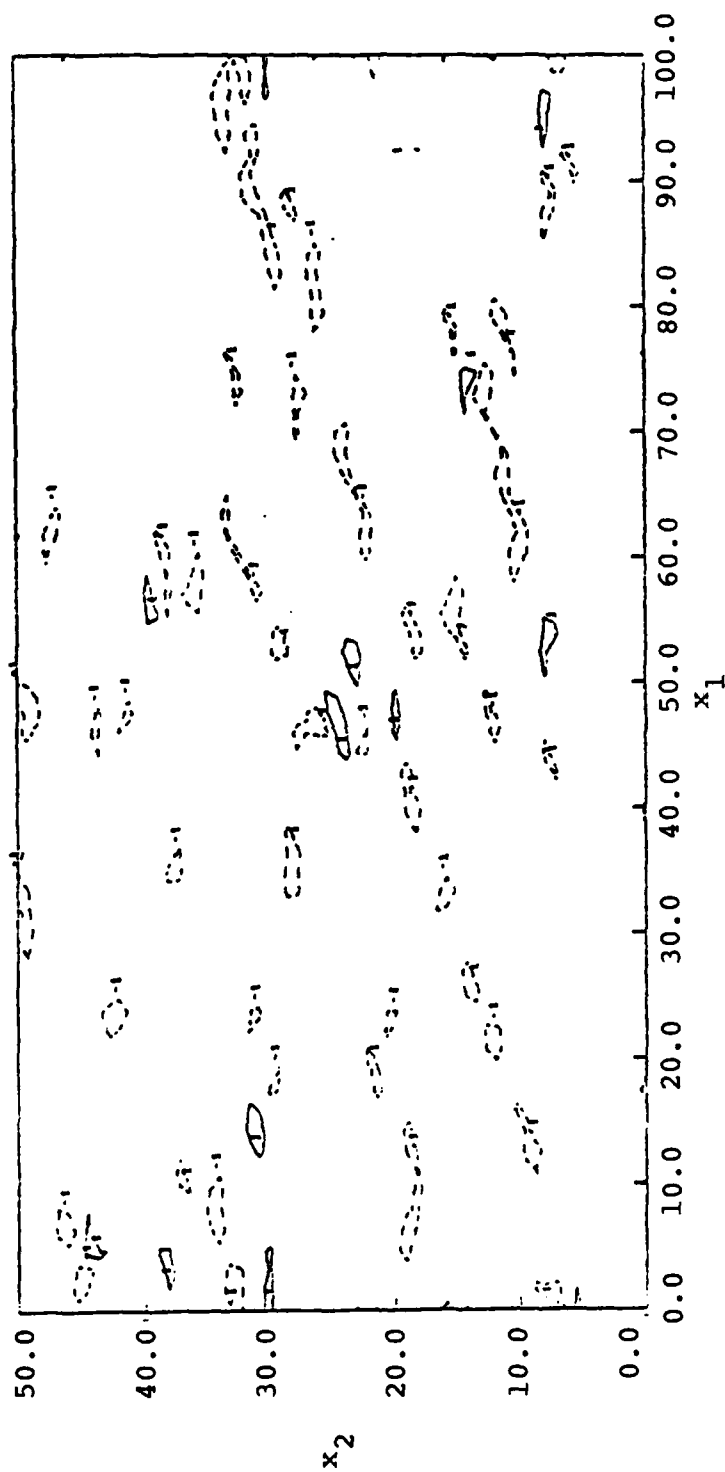
Figure 5. Contours of the fluctuating spanwise vorticity in the x_1-x_2 plane for the flow shown in Figures 1-4. The plane is the one shown in Figures. 3 and 4.

-42-

Total Strain, St
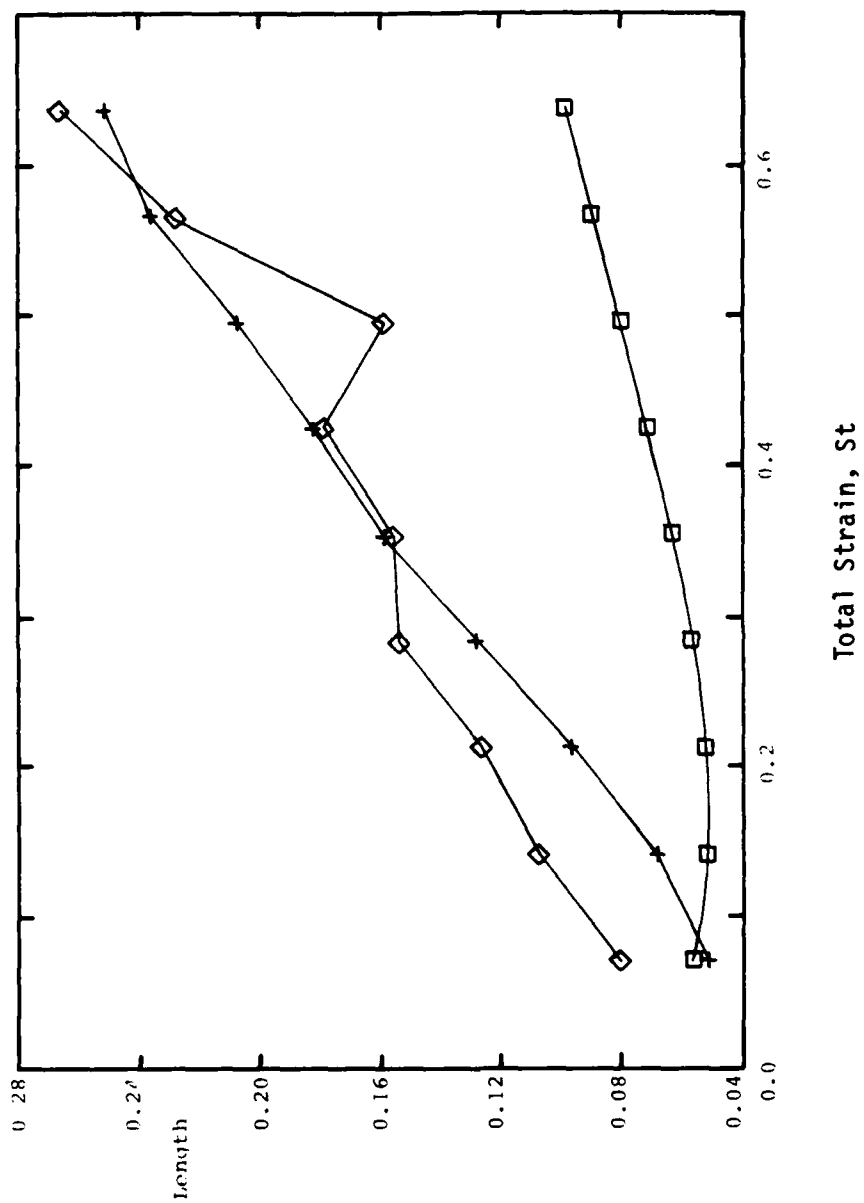
Figure 6. The integral length scale ($\diamond$), dissipation length scale (q^3/ϵ)/10
(+), and mixing length ($\square$) as functions of the total shear in
homogeneous shear flow. Data shown are for Case BSH9 from Rogallo
(1981); the other cases are qualitatively similar.

-43-
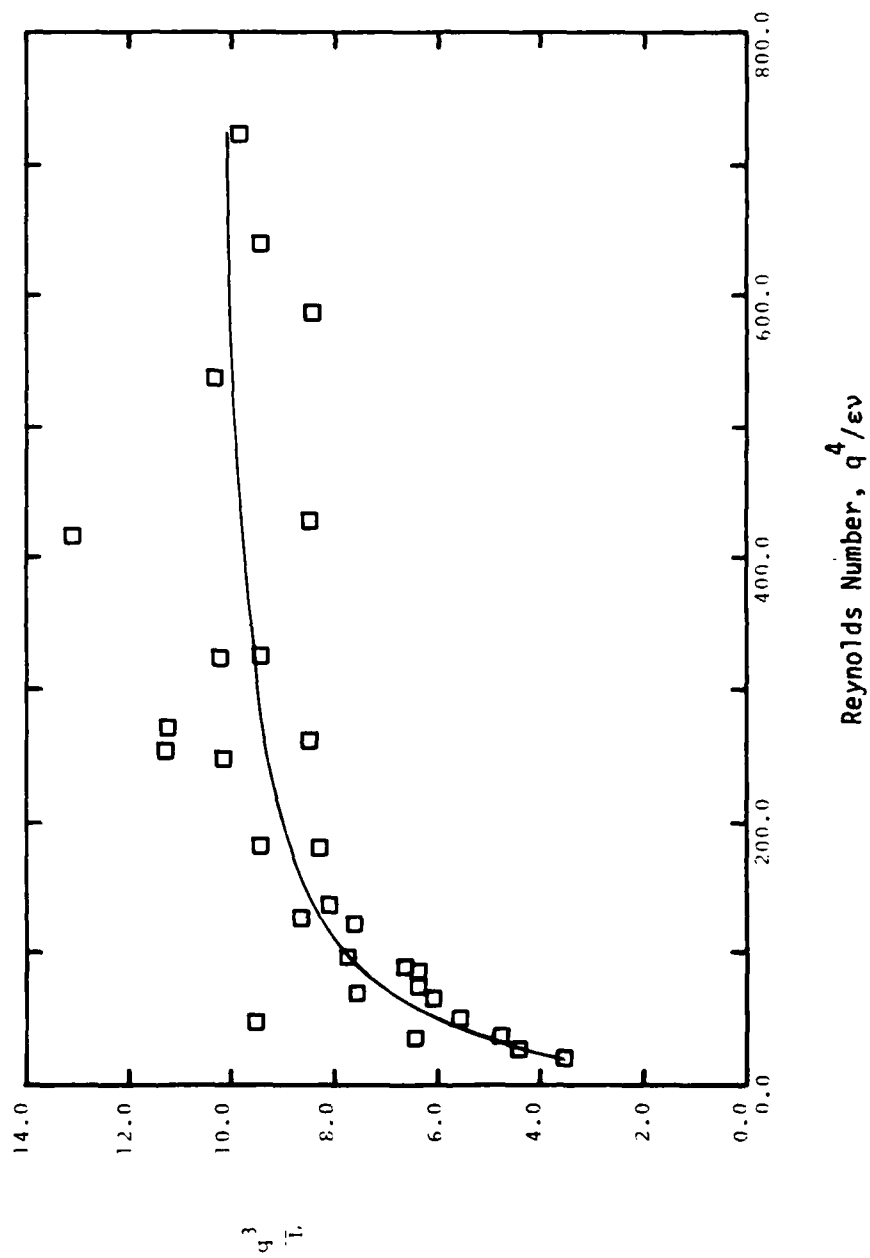
Reynolds Number, $q^4/\epsilon\nu$

Figure 7.   The ratio of the dissipation length scale to the integral scale as a function of the Reynolds number $q^4/\epsilon\nu$ for the homogeneous shear flow cases.   The smooth curve is the fit given by Eq. (7).
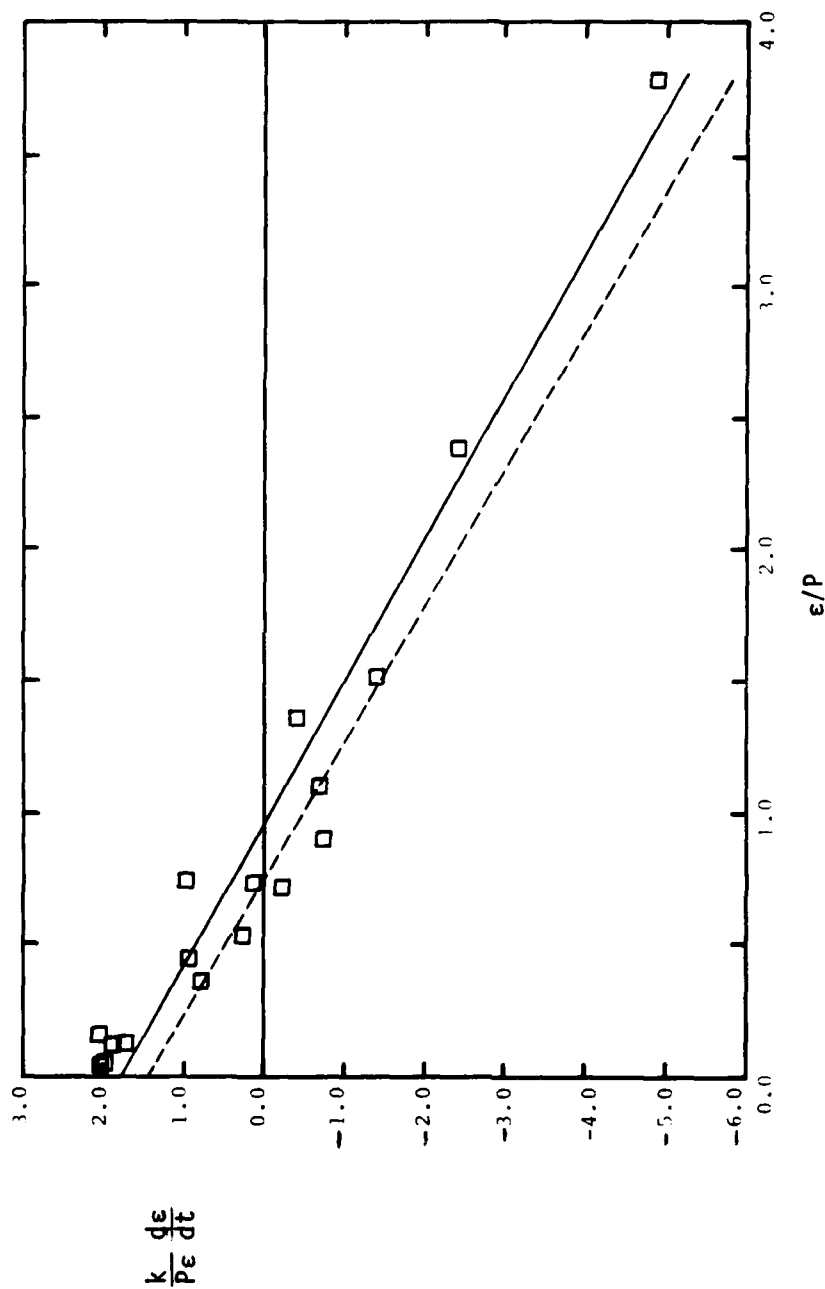
Figure 8. A test of the modeled dissipation equation for turbulence under-going homogeneous plane strain. Full simulation data for $(k/\epsilon P)d\epsilon/dt$ are plotted against the ratio of dissipation to production; the model expects the data to fall on a straight line. Also shown are the least squares fit to the data and the prediction of the standard model; the parameters are given in Table 9. □ = data; —— = least squares fit; ---- = standard model.
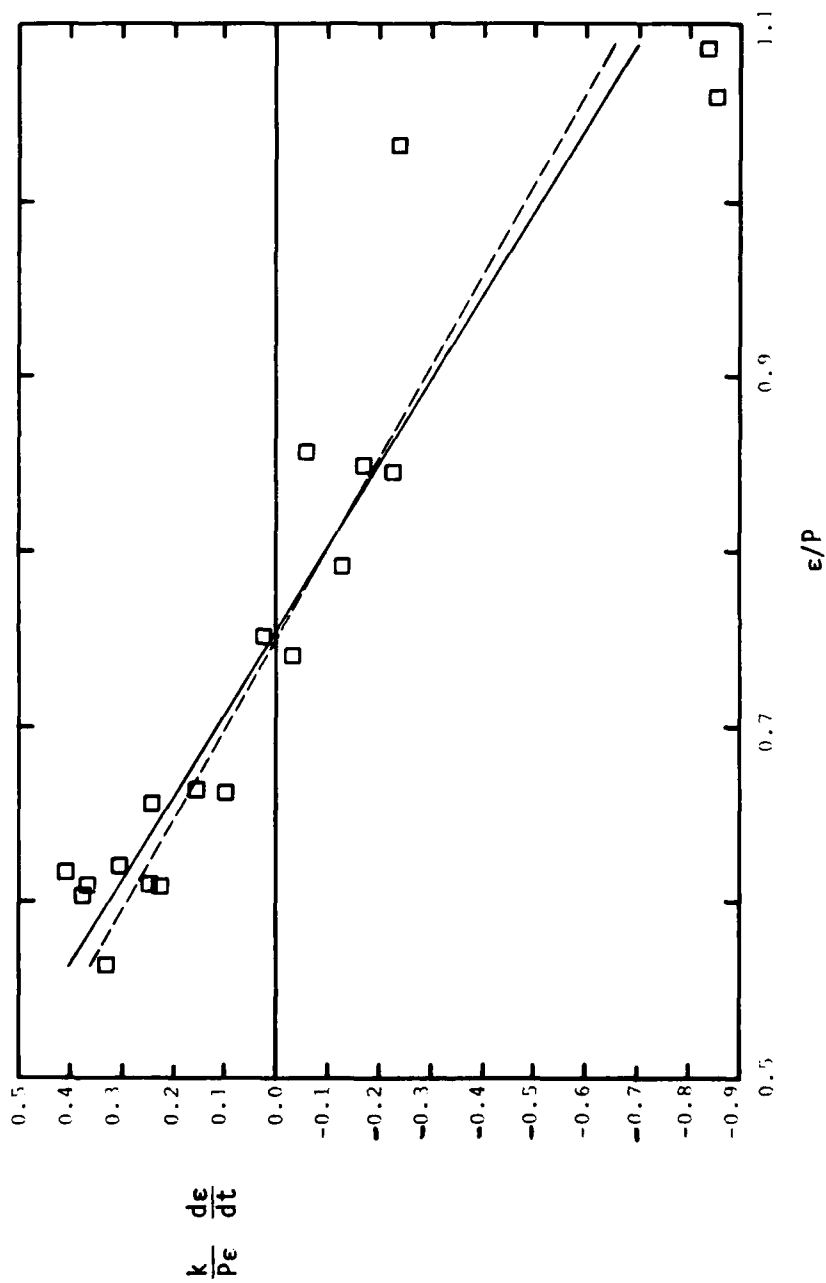
Figure 9. A test of the modeled dissipation equation for turbulence
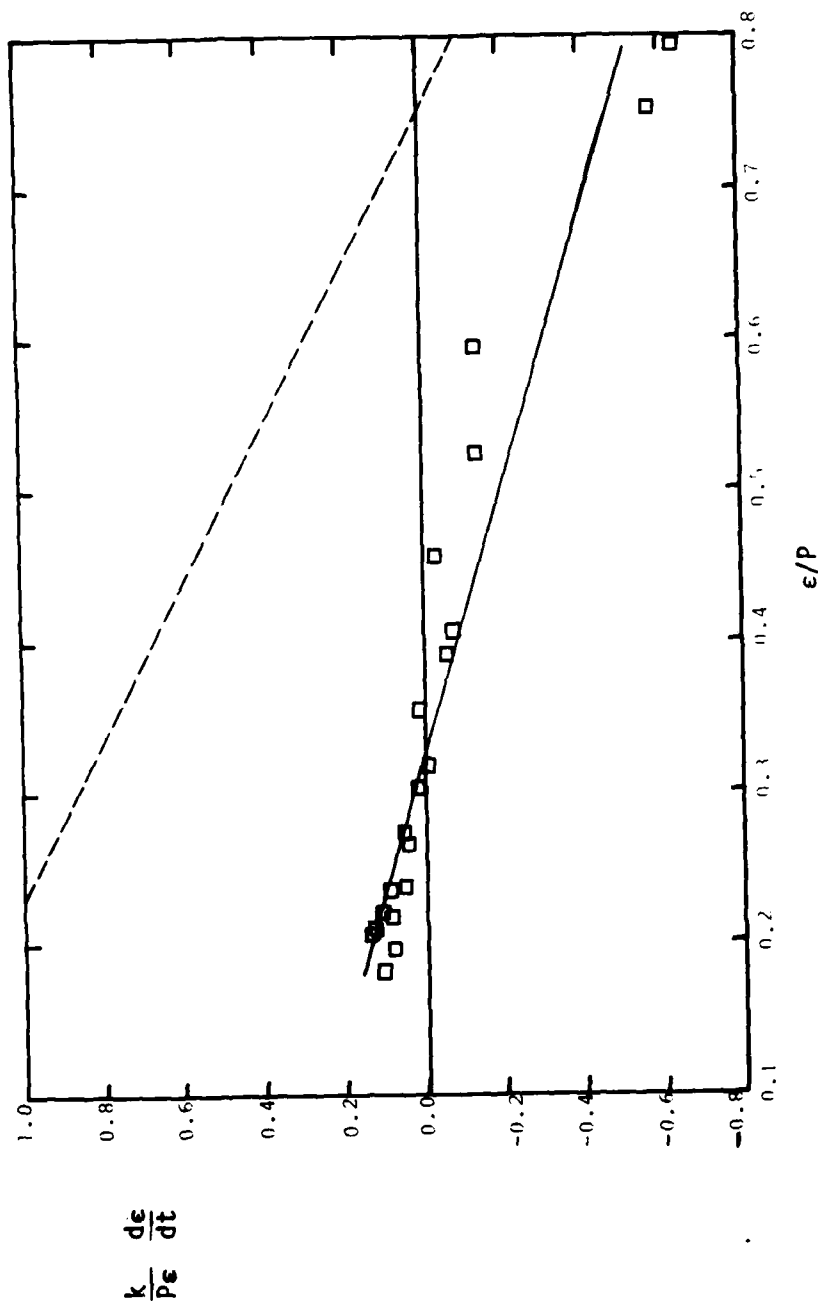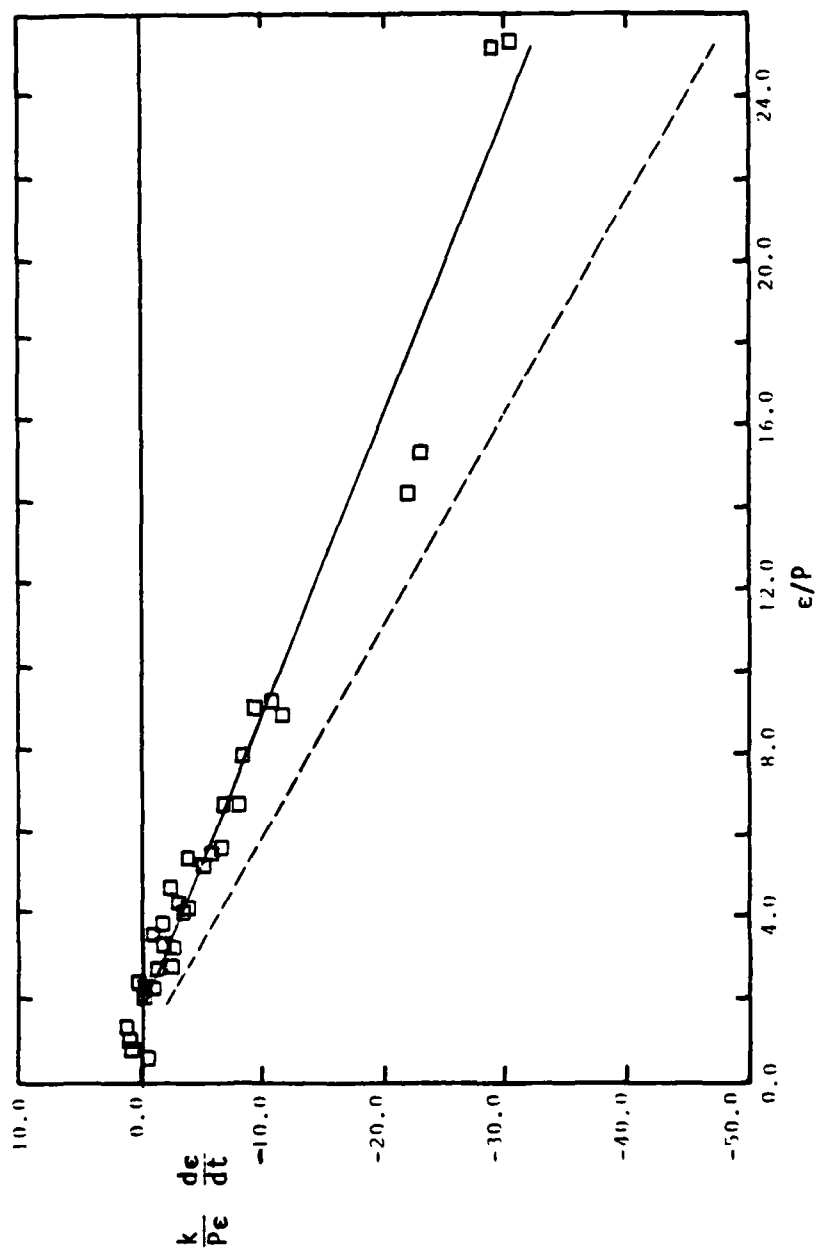undergoing homogeneous shear. See Figure 8 for a detailed
description.
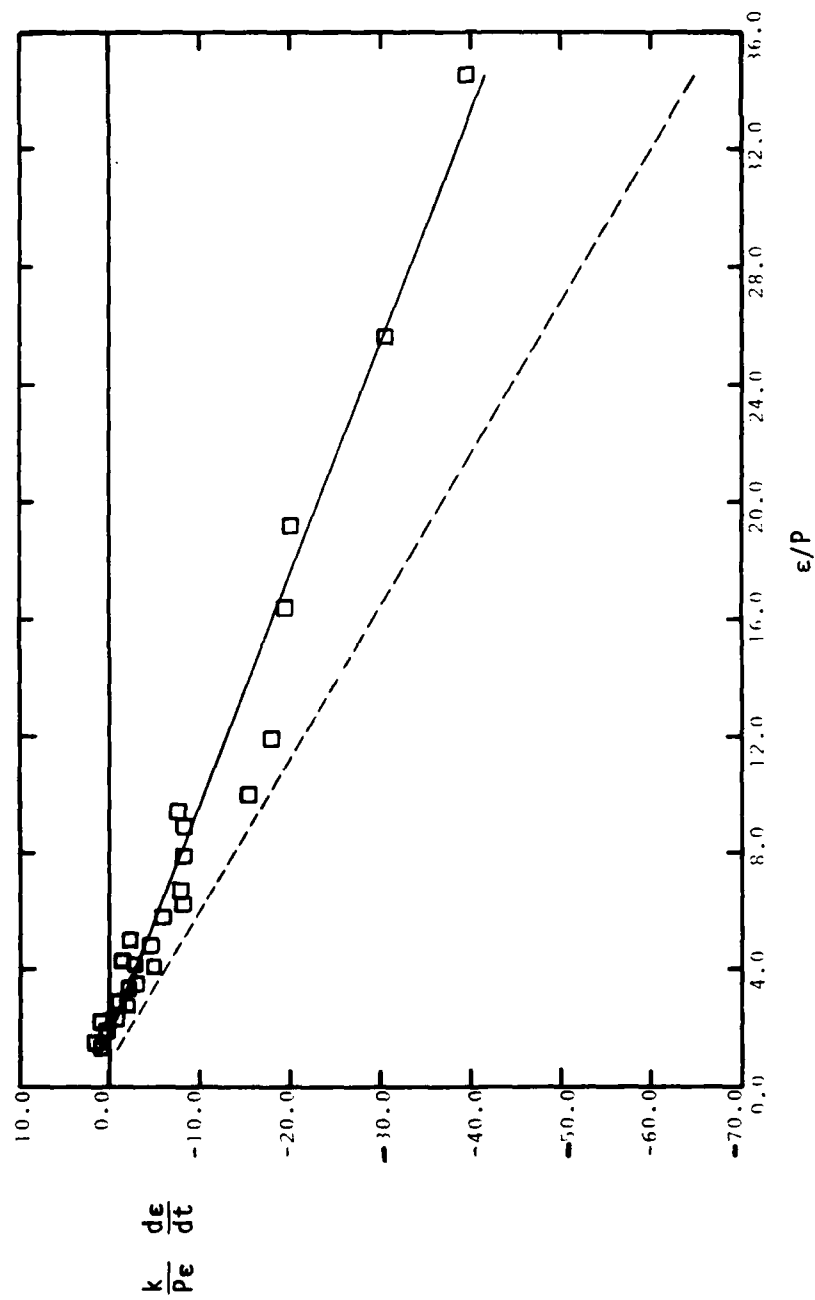
Figure 10. A test of the modeled dissipation equation for turbulence undergoing homogeneous axisymmetric strain. See Fig. 8 for a detailed description.
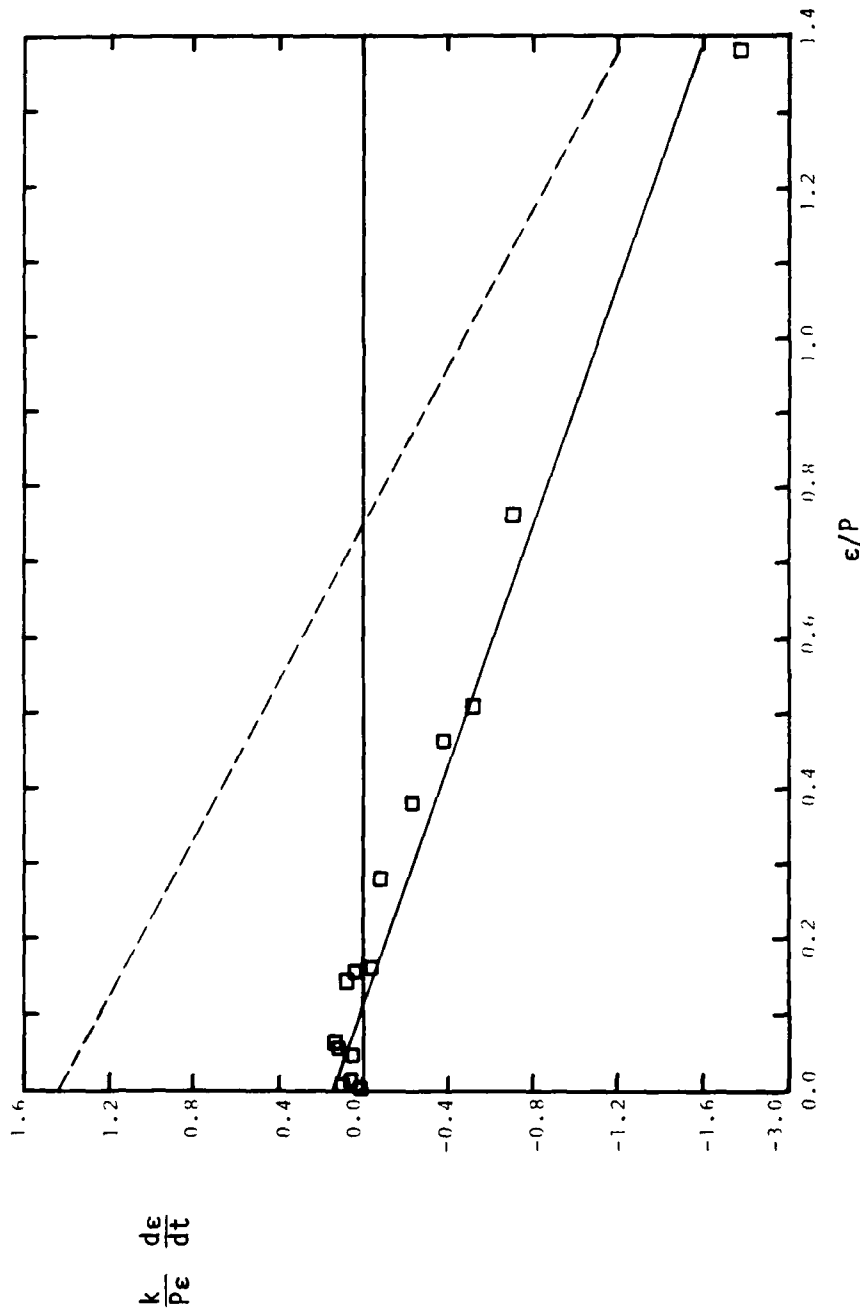
Figure 11. A test of the modeled dissipation equation for turbulence undergoing homogeneous plane strain. Data for $(K/\epsilon P)d\epsilon/dt$ derived from the modeled production given by Eq. (11) are plotted against the ratio of dissipation to production; the model expects the data to fall on a straight line. Also shown are the least squares fit to the data and the prediction of the standard model; the parameters are given in Table 9. Symbols are the same as in Figure 8.

Figure 12. A test of the modeled dissipation equation for turbulence undergoing homogeneous axisymmetric strain. See Figure 11 for a detailed description.

-49-

Figure 13. A test of the modeled dissipation equation for turbulence undergoing homogeneous axisymmetric strain. See Figure 11 for a detailed description.
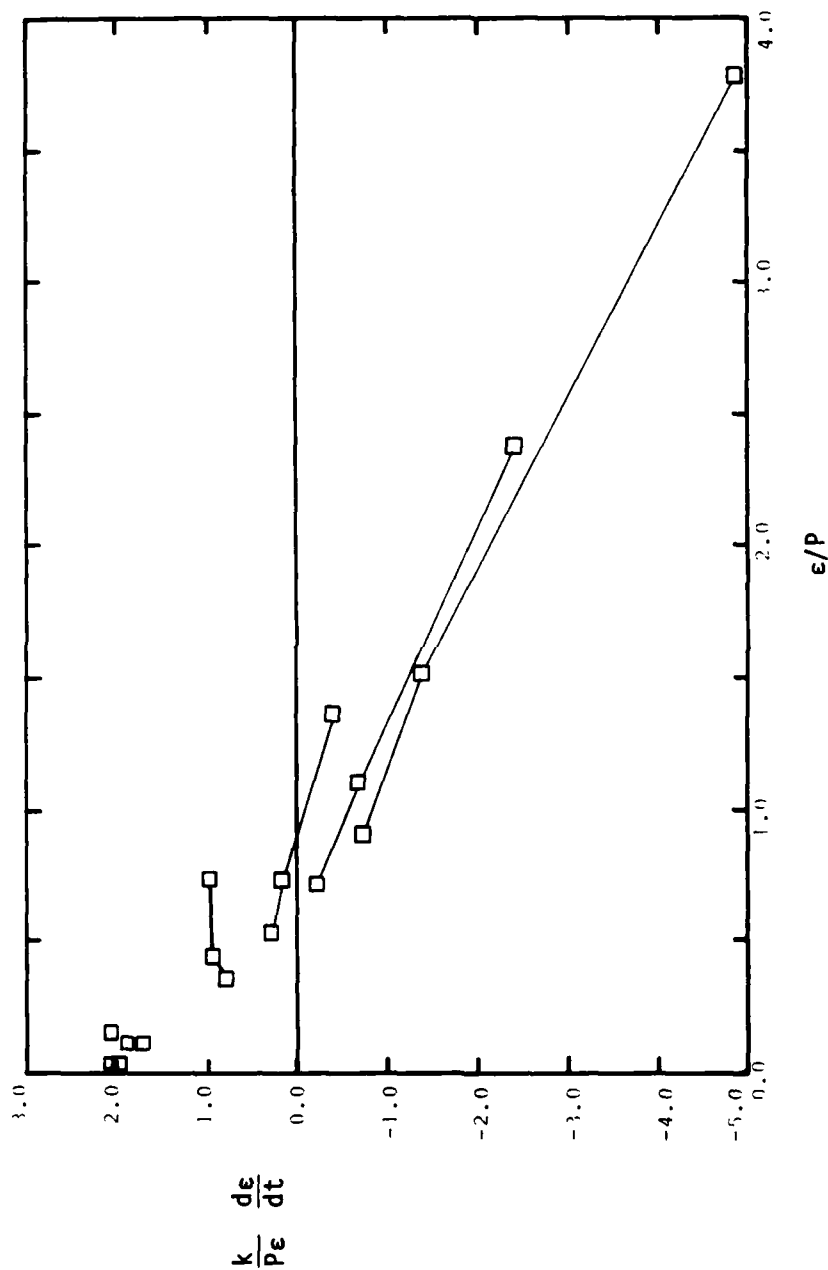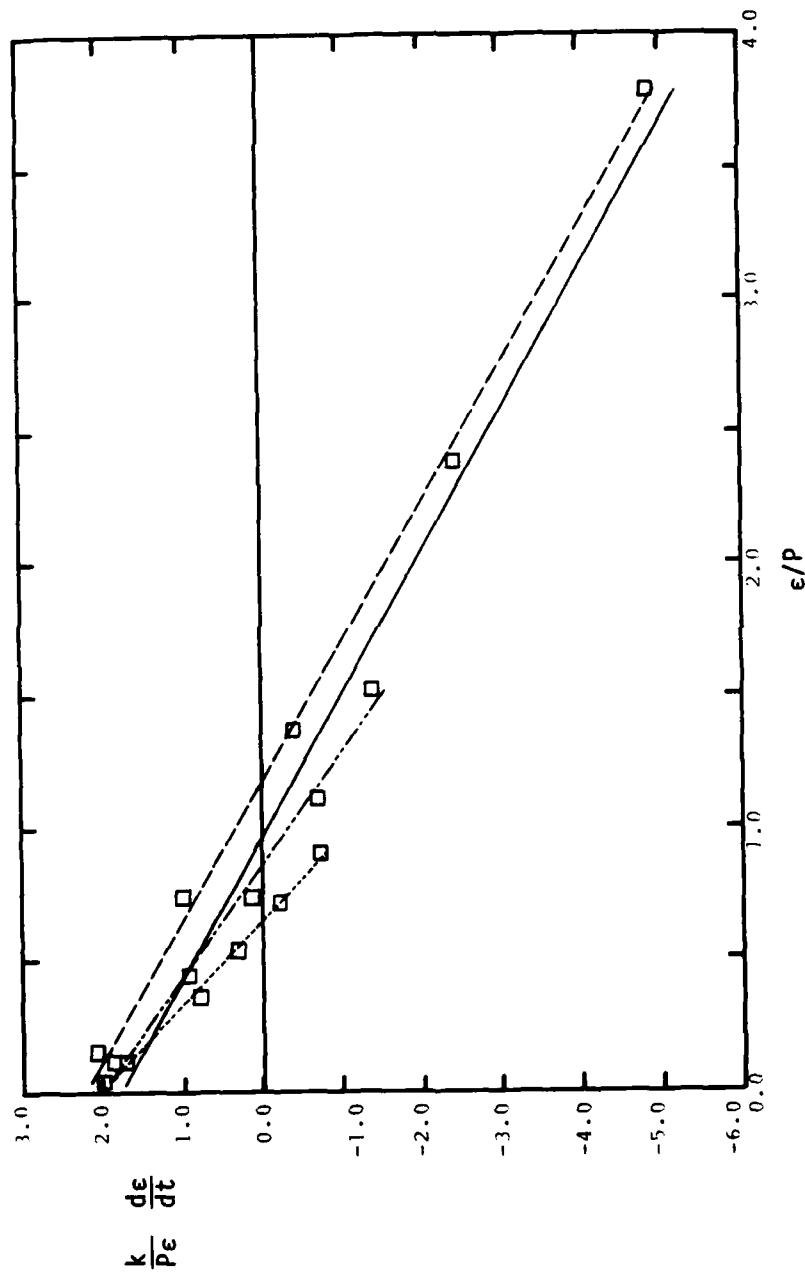
Figure 14. Full simulation data for $(k/\epsilon P)d\epsilon/dt$ plotted against the ratio of dissipation to production for turbulence undergoing homogeneous plane strain. This plot is identical to Figure 8 but the lines represent the data for particular runs.

-51-

Figure 15. Full simulation data for $(k/\epsilon P)d\epsilon/dt$ plotted against the ratio of dissipation to production for turbulence undergoing homogeneous plane strain. This plot is identical to Figure 8 but the lines represent the data for fixed values of the total strain:
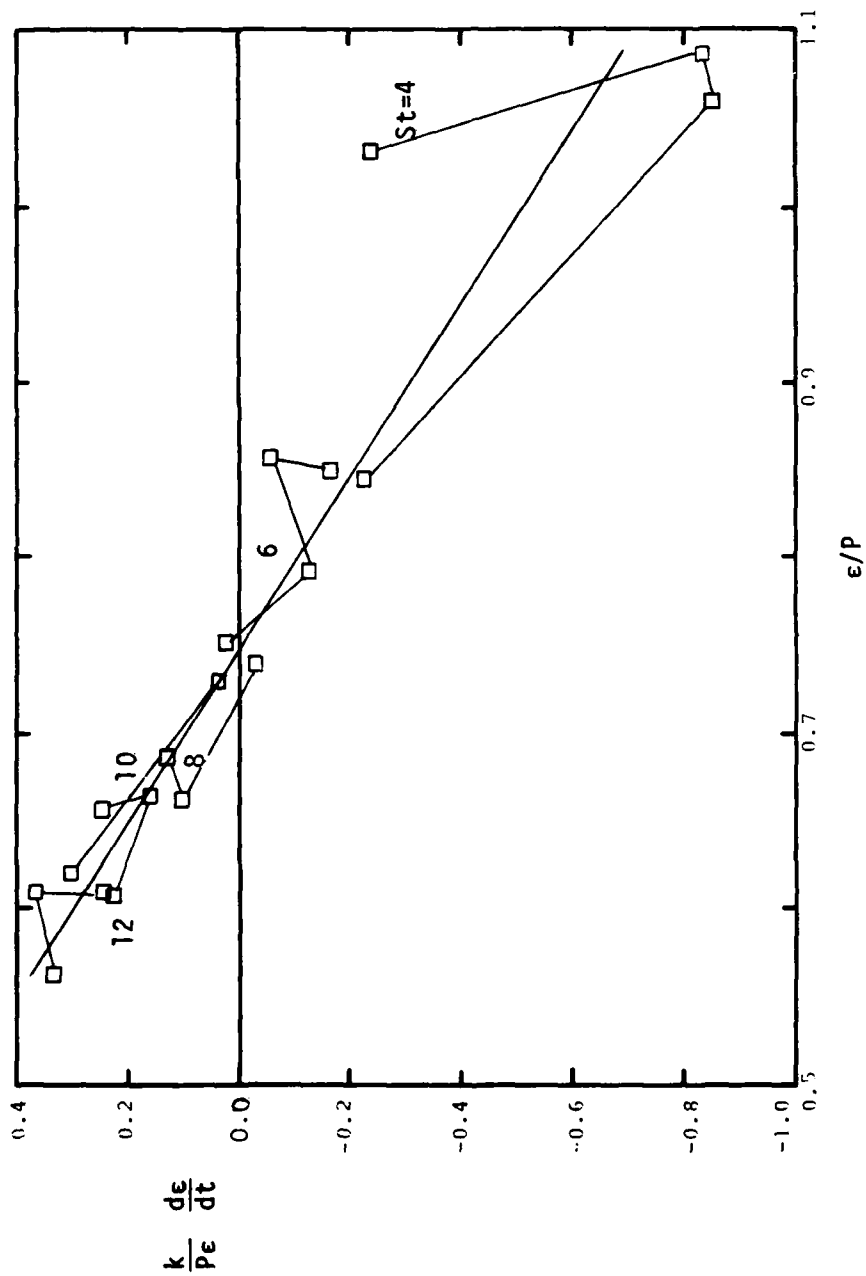---- St = 1.05, ── ·── St = 0.7, ── ── St = 0.35, ── overall fit.

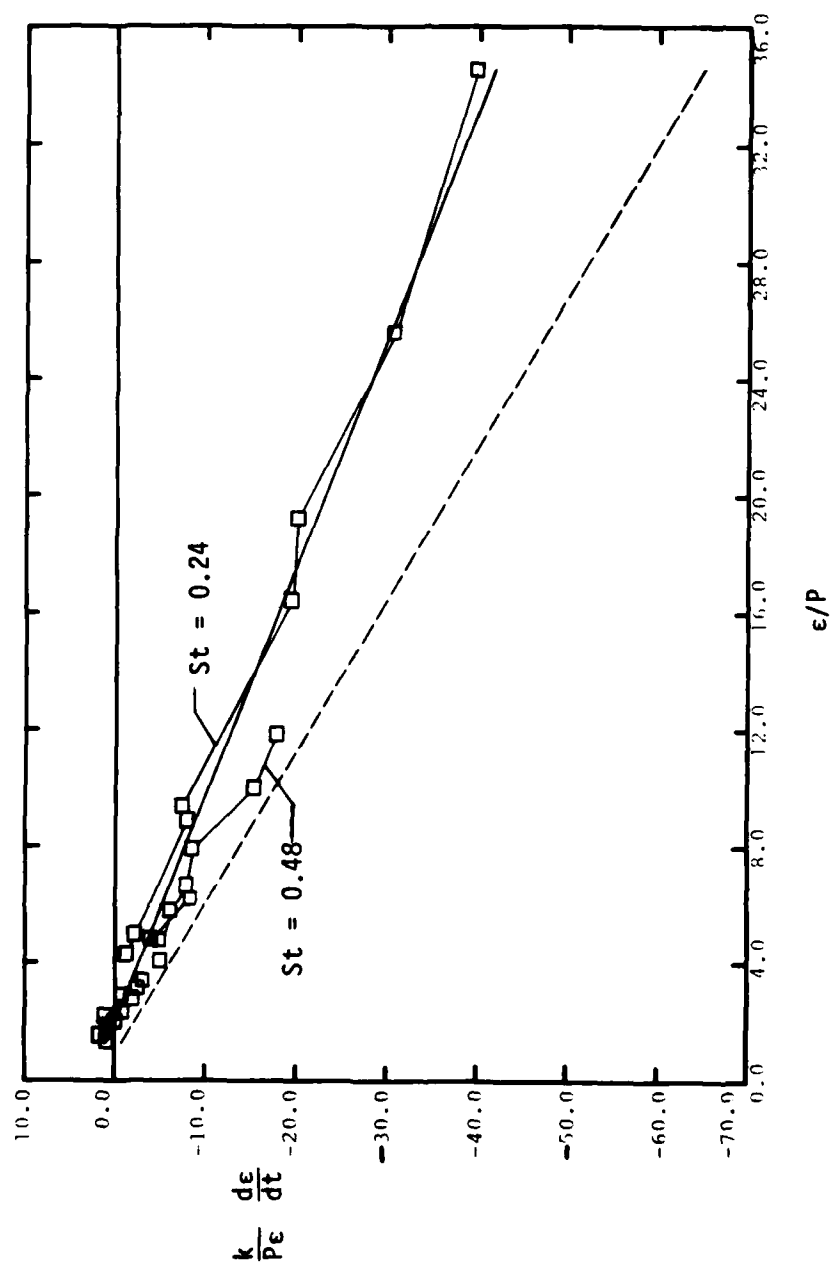Figure 16. A plot similar to Figure 15 but for turbulence undergoing homogeneous shear.

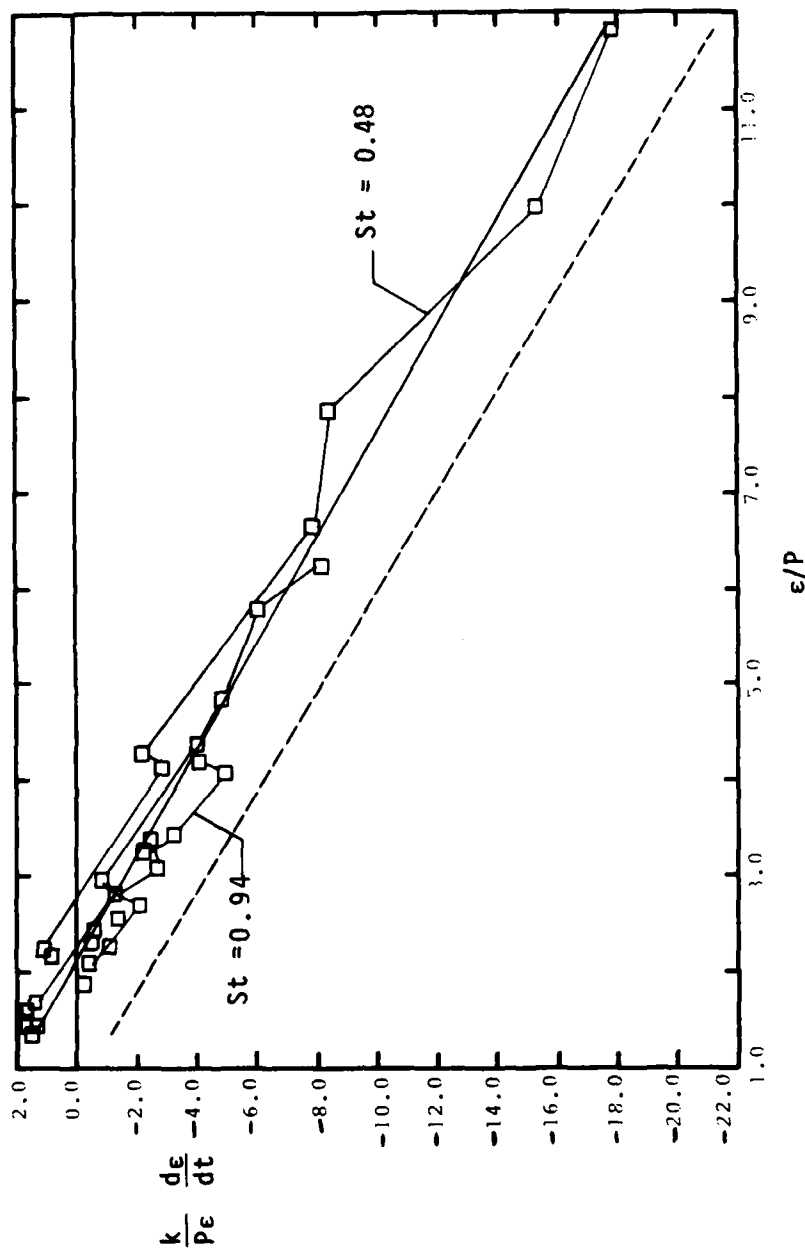Figure 17.   A plot similar to Figure 15 but for turbulence undergoing axsymmetric strain.

Figure 18. This plot is identical to Figure 17 except that the data for St = .24 have been eliminated.

END

FILMED

5-85

DTIC